Seismological Research Letters

RAMONES, the Rapid Assessment of MOmeNt and Energy Service in Central Italy: Concepts, capabilities and future perspectives

--Manuscript Draft--

Manuscript Number:	
Full Title:	RAMONES, the Rapid Assessment of MOmeNt and Energy Service in Central Italy: Concepts, capabilities and future perspectives
Article Type:	Focus Section - European Seismic Networks
Corresponding Author:	Daniele Spallarossa Dip.Te.Ris Univ. of Genoa (Italy) Genoa, ITALY
Corresponding Author Secondary Information:	
Corresponding Author's Institution:	Dip.Te.Ris Univ. of Genoa (Italy)
Corresponding Author's Secondary Institution:	
First Author:	Daniele Spallarossa
First Author Secondary Information:	
Order of Authors:	Daniele Spallarossa
	Matteo Picozzi
	Davide Scafidi
	Paola Morasca
	Chiara Turino
	Dino Bindi
Order of Authors Secondary Information:	
Manuscript Region of Origin:	ITALY
Suggested Reviewers:	Domenico Di Giacomo domenico@isc.ac.uk
	Alberto Michelini alberto.michelini@ingv.it
	Emeline Maufroy emeline.maufroy@univ-grenoble-alpes.fr
	Zafeiria Roumelioti zroumelioti@upatras.gr
Opposed Reviewers:	

The RAMONES service for rapid assessment of seismic moment and radiated energy in central Italy: concepts, capabilities and future perspectives

Daniele Spallarossa (1,2), Matteo Picozzi (3), Davide Scafidi (1), Paola Morasca (2), Chiara Turino (1) and Dino Bindi (4)

(1) University of Genoa, DISTAV, Genoa, Italy
(2) Istituto Nazionale di Geofisica e Vulcanologia (INGV), Milan, Italy
(3) University of Naples Federico II, Department of Physics, Naples, Italy
(4) Helmholtz Centre Potsdam, GFZ German Research Centre for Geosciences, Potsdam, Germany

Corresponding author:
Daniele Spallarossa,
Dipartimento di Scienze della Terra dell'Ambiente e della Vita (DISTAV),
University of Genoa, Viale Benedetto XV 5, 16132 Genoa, Italy
daniele.spallarossa@unige.it

Abstract

We present RAMONES, a service for disseminating through a web-interface, the estimates of seismic moment (M_0) and radiated energy (E_R) for earthquakes occurring in central Italy with local magnitude above 1.7. The service is based on an a fully-automatic procedure developed for downloading and processing open seismological data from the European Integrated Data Archive – EIDA, from the Italian Civil protection (DPC) repository, and from Incorporated Research Institutions for Seismology-IRIS. In its actual configuration, RAMONES uses the seismic catalog generated through the event web-service of the Italian Institute of Geophysics and Volcanology to guide the data download. The concept of RAMONES is to estimate M_0 and E_R from features extracted directly from recordings, namely the peak displacement (PD_S) and the integral of the squared velocity ($IV2_S$) evaluated over the S-wave window at local distances. A data set composed by 6515 earthquakes recorded in central Italy between 2008 and 2018 has been used to calibrate the attenuation models relating M_0 to PD_S and E_R to $IV2_S$, including station corrections. The calibration values for M_0 and E_R have been extracted from the source spectra obtained by applying a decomposition approach to the Fourier amplitude spectra known as generalized inversion technique. To test the capabilities of RAMONES, we validate the attenuation models by performing residual analysis over about 60 earthquakes occurred in 2019 that were used for the spectral decomposition analysis but not considered in the calibration phase. Since January 2020, a testing operational phase is running and RAMONES analyzed about 800 earthquakes by September 2020. The distribution of the source

parameters and their relevant scaling relationships are automatically computed and disseminated in form of maps, parametric tables, figures, and reports available through the RAMONES web-interface.

Introduction

The long history of destructive earthquakes in Europe, where also moderate events can have tremendous effects due to the high density of populated areas and the high vulnerability of historical cities and settlements, led the seismological community to establish, in 1987, the Observatories and Research Facilities for European Seismology, ORFEUS (Nolet et al., 1986). The standardization of formats for data transmission and archiving (FDSN, see Data and Resources) and the establishment of open repositories for sharing real time and archived streams (e.g., IRIS and EIDA, see Data and Resources) had a strong impact on opening new scientific directions. If the development in data telemetry opened the new research field of real-time seismology (Kanamori 2005), the availability of denser and high quality seismic networks deployed near faults, made possible to record very large numbers of micro and-small earthquakes, pushing the seismological community to develop novel big data analysis strategies (e.g., Ross et al., 2017; Zhu and Beroza, 2018; Ross et al., 2019; Kong er al., 2019; Mousavi et al., 2109a; Mousavi et al., 2109b; Munchmeier et al., 2019; Scafidi et al., 2019). Within the current operational scenario where large volume of data from dense seismic networks can be fast accessed and processed, the development of services for rapid assessment of source parameters became feasible. Here, we present a service providing seismological products for characterizing the seismic source properties in Central Italy, named RAMONES ('Rapid Assessment of MOmeNt and Energy Service'). In its actual configuration, RAMONES uses information and data provided by services of the Italian Civil Protection Department (DPC) and of the European Integrated Data Archive (EIDA) to disseminate, among other parameters, estimates of the seismic radiated energy (E_R) and seismic moment (M_0) for earthquakes larger than M_L ~1.7 in central Italy. The parameters are computed using features extracted directly from recordings and the outcomes are disseminated with an a-priori fixed delay of one day with respect to the earthquake origin time. The need to develop a monitoring strategy for earthquake source parameters originated after the 2016-2017 Central Italy seismic sequence that included three mainshocks (i.e., the Mw 6.2 Amatrice, Mw 6.1 Visso, and Mw 6.5 Norcia earthquakes occurred between August 24th and October 30th, 2016), and lead to record more than 500.000 earthquakes till mid 2017 (e.g., Zhang et al., 2019; Spallarossa et al., 2020). RAMONES builds its strategy for the rapid and robust assessment of M_0 and E_R over previous studies performed in central Italy. For earthquake early warning purposes, Picozzi et al. (2017) proposed the estimation of the radiated seismic energy and seismic moment from P-wave signals for almost 40

earthquakes, including the largest magnitude events of the 2016-2017 Central Italy seismic sequence. The authors showed that it was possible, by comparing the moment and the energy magnitude scales, to identify events with stress drop higher than the average, providing an important information about the earthquake shaking potential. A further development was proposed by Bindi et al. (2018), who focused on S-wave windows of more than 1400 earthquakes in the magnitude ranges $2.5 \leq Mw \leq 6.5$, recorded by local networks in Central Italy from 2008 to 2017. The authors used their estimates of both E_R and M_0 to investigate the impact of different magnitude scales on the aleatory variability associated with regional ground motion prediction equations (Bindi et al., 2019). In this study, we review the procedure for estimating M_0 and E_R from S-wave windows, enlarging the calibration data set. Most importantly, the scientific algorithms are re-engineered to work automatically and to provide outcomes through a web-application as presented in the following sections.

RAMONES web-interface

RAMONES (Rapid Assessment of MomeNt and Energy Service) is a service for disseminating seismic moment (M_0) and radiated energy (E_R) computed by applying empirical attenuation models to features extracted from recordings. The service, available at the link http://www.distav.unige.it/rsni/ramones.php, is active since January 2020, providing the source parameters for earthquakes with local magnitudes M_L larger than about 1.7 recorded within a region bounded by 40.0°N and 44.5°N in latitude and 10.50°E and 16.50°E in longitude. The threshold magnitude has been selected following Bindi et al. (2020). These authors analyzed a subset of data considered in this study and found that, given the stations azimuthal and distance distribution in the investigated area, reliable source parameters can be retrieved for earthquakes above Mw 1.8-2, without strong bias due to unaccounted attenuation effects.

RAMONES is based on an automatic procedure implemented through the following steps: 1) locations and magnitudes of earthquakes occurred within the target region are retrieved from the INGV (National Institute for Geophysics and Volcanology) bulletin (see Data and Resources); 2) Hypocentral information are used to extract segments from continuous data streams archived by EIDA (European Integrated Data Archive) and in the DPC (Department of Civil Protection) repository; only recordings at hypocentral distances shorter than 120 km are downloaded, along with the relevant station metadata. 3) The automatic procedure described in Scafidi et al. (2016) is applied to detect P and S onsets, to estimate the local magnitude and to extract different features from the recordings, such as: the peak displacement and the integrated squared velocity over the S-wave

window, the peak ground velocity (PGV) and acceleration (PGA). 4) the seismic moment (M_0) and radiated energy (E_R) are estimated using empirical attenuation models derived in this study, and described in the following sections. Furthermore, additional parameters such as apparent stress (σ_a; Wyss and Brune, 1968) and the moment magnitude (M_W, Hanks and Kanamori, 1979) are computed as well. 5) Finally, the results are stored in a PostgresSQL database and disseminated through a web interface. In its actual configuration, RAMONES updates are scheduled on daily basis.

A web portal allows the users to interact with the database. The main page of RAMONES (Figure 1) includes:

- A map of the monitored region showing the epicenters of earthquakes processed by RAMONES since January 2020. Using the "Change selection" option, the geographical extension, the depth and magnitude ranges, and the time span of interest can be configured by the user. In its actual configuration, RAMONES analyses earthquakes with magnitude above M_L 1.7 occurring in central Italy.

- Selecting "Seismic station", RAMONES shows a table reporting the main information of the stations stored in the database and actually used by the service (more than 550 at 15/09/2020). In particular, the table includes:

  - Station information (Code, network, channels, latitude, longitude, elevation and location) including links;
  - Link to medatata (dataless);
  - Link to an automatically generated summary document (Pdf) showing a map with the station location and H/V spectral ratios for both S−wave phase window and noise window computed by the service.
  - Tools for searching, sorting, and exporting the station table are also implemented.

- A table reporting the main information of the earthquakes stored in the RAMONES database and the associated source parameters. In particular, the table includes:

  - The earthquake location (Origin time, latitude, longitude, depth) provided by the INGV bulletin and a link (ID-INGV) to the INGV event-specific web-page;
  - The base-10 logarithm of the estimated seismic moment, Log(M_0), and radiated energy, Log(E_R). The empirical attenuation models used to compute these parameters are

described in the following sections;

- Several magnitude estimates are listed: ML_{INGV} and Mw_{INGV} are the local and moment magnitudes reported by the INGV bulletin; ML_{IT16} is the local magnitude computed considering the attenuation model of Di Bona (2016), but without considering the station corrections: ML_{IT16}= Log(A)+1.667Log(R/100)+0.001736(R-100)+3, where A is the geometrical mean of the two horizontal Wood-Anderson amplitudes in mm, and R the hypocentral distance; Mw is the moment magnitude computed from our M_0 estimates using Hanks and Kanamori (1979): Mw = (Log(M_0)-9.1)/1.5; ML_{ER} is a local magnitude calibrated over Log (E_R), similarly to Picozzi et al. (2018), as described in the following sections;
- The apparent stress σ_a (Wyss and Brune, 1968) is computed assuming a constant rigidity (μ) in the source area equal to 3×10^4 MPa, considered as representative of the average crust conditions for the central Apennines chain.
- Finally, the first three columns provide an additional link to the event-specific page (Region), to a static image showing few selected recordings (Waves) and to an automatically generated summary document (Pdf).

- Tools for searching, sorting, and exporting the event table are also implemented.
- Below the event table, five different figures are automatically updated to summarize the scaling relationships among different source parameters (e.g., scaled energy E_R/M_0 versus Mw; Log(E_R) versus Log(M_0); ML_{ER} versus ML_{IT16}). Each panel reports both the values used to calibrate and validate the empirical models (i.e., events occurred before 2020) and those obtained by applying the models to earthquakes occurred after the calibration phase.

Through the link in the first column (Region), an event-specific page for the selected event is opened (Figure 2). This page provides a map with the location of stations used by RAMONES for the processing and the earthquake location; a summary of the source parameters of the selected events; a table listing several information extracted from each recordings: the station and network names, the specific channel (using the SEED convention for the channel names; see Data and Resources); the hypocentral distance; the station local magnitude; the peak ground acceleration (PGA) and velocity (PGV) over the three components; the station estimates of Log(M_0), and Log(E_R); a flag (Used) to indicate whether a record has been used (X) or discarded (-) for the event magnitude calculation (i.e., discarded records have low signal-to-noise ratio). Finally, it is also possible to download the

information contained in the event-specific page into a document (PDF) (the same document that can be download from the table in the main page) and to visualize the waveforms of the vertical component recorded at the 10 closest stations.

Data and processing

The data set used to calibrate the empirical models used by RAMONES consists of 6515 earthquakes located in central Italy (Figure 3) and recorded by 464 stations. This data set includes broad-band, short period and accelerometric signals recorded since 2008. The bulk of the data set originates from 2016-2017 central Italy sequence (Chiaraluce et al., 2017) and 2009 Aquila sequence (Ameri et al., 2009). Data for calibration have been collected by the following permanent networks: The National Seismic Network (RSN), operated by INGV, Mednet operated by INGV and the National Accelerometric Network, RAN, operated by the Department of Civil Protection (see Data and Resources). Stations from temporary networks were also used for calibrating the attenuation models. These include the networks for aftershock monitoring (Margheriti et al., 2011), for site effects (Bergamaschi et al., 2011; Cultrera et al., 2016) and for seismic microzonation (Working Group SM-AQ, 2010; Cara et al., 2019).

The selected data set is composed by almost 840000 waveforms (considering the three components of motion) in the M_L range 1.6 – 6.5 (Figure 4a). The hypocentral distances span the range 5-150 km, with about 50% of the data recorded at hypocentral distances < 30 km. Depth shows a bimodal distribution, with peaks at about 3 km and 7.5 km (Figure 4b). Broad-band seismometers (i.e., channel HH) and short period seismometers (channel EH) are often co-located with strong motion sensors (channel HN) and the distributions with distance of the number of recordings for the different channels are shown in Figure 4c. In this study, co-located instruments are considered as different stations. Details on instruments and stations of each network are listed in Table 1S in the supplement materials. About 50% of the stations recorded at least 40 earthquakes and about 50% of the earthquakes has at least 40 records (Figure 4d). Data selection and processing is made following Pacor et al. (2016) and Bindi et al., (2018). In particular, an automatic procedure (Spallarossa et al 2014; Scafidi et al., 2016) is applied for determining the P and S-wave onsets and the earthquake location is performed with a non-linear location algorithm (Lomax et al., 2000), considering a 1D velocity model calibrated for the area with station corrections (Spallarossa et al., 2020).

Aiming to have consistent estimates of the local magnitude for the whole data set, Wood-Anderson seismograms in the hypocentral distance range 10-100 km are synthesized following Spallarossa et al. (2002). The local magnitude ML_{IT16} is then computed by averaging the station magnitude estimates and considering the zero-magnitude attenuation model calibrated by Di Bona (2016) for Italy, but without applying station corrections. Figure (5) shows the RAMONES processing workflow used to evaluate, for each recording, the S-wave peak displacement (PD_S) and the integral of the squared velocity ($IV2_S$) over the S-wave window. The workflow is based on procedure developed by Scafidi et al. (2019). The high-pass corner frequency of the pre-deconvolution filter is automatically determined based on signal-to-noise analysis, selecting the lowest frequency in the 0.3 – 2.0 Hz range for which the signal-to-noise ratio is larger than 4.0. The parameters PD_S and $IV2_S$ are computed considering a time window starting 0.1 s before the S-wave onset and ending at different percentages of the cumulated energy as a function of the source to site distance R: (i) 90 per cent when $R < 25$ km; (ii) 80 per cent when $25 \text{ km} < R < 50$ km; (iii) 70 per cent when $R > 50$ km. For both PD_S and $IV2_S$ calculation, we imposed a minimum time window length of 2.5 s and a maximum time window length of 20 s. For each recording, a signal-to-noise ratio was evaluated considering a pre-event noise window of the same length as the direct S-waves. The logarithm of both PD_S and $IV2_S$ are computed using displacement and velocity band-pass filtered signals: the low-pass and high-pass corner frequencies are computed by signal-to-noise ratio (SNR) analysis. For calibrating the empirical model describing the scaling of PD_S with hypocentral distance and M_0 , the estimates of PD_S for the NS and EW components are averaged (geometric mean). For the scaling of $IV2_S$ with hypocentral distance and E_R , the measures of $IV2_S$ obtained the three components of ground motion are summed up. Figure (6a) and (6b) show the distribution of PD_S and $IV2_S$ with respect to hypocentral distance, respectively. Finally, the Fourier Amplitude Spectra (FAS) are calculated and selected following the procedure described in Pacor et al. (2016).

RAMONES concept

The concept developed for the rapid assessment of M_0 and E_R relies on measuring specific ground motion features directly on seismograms and to correct them for propagation and site effects using empirical models previously calibrated for the region of interest. The source parameters needed to derive the attenuation models are extracted from the FAS of the 6515 earthquakes selected from the central Italy dataset and by applying a spectral decomposition approach known as generalized inversion technique (GIT) (among others, Andrews, 1986; Castro et al., 1990; Oth et al., 2011). The GIT assumes that the recorded spectra are given by the convolution of source, propagation and site

terms; a factorization of the spectra, expressed as inverse problem, is possible by exploiting the redundancy of information available when the same event is recorded by different stations located at different distances and the same station is recording several different earthquakes. We apply the GIT in its non-parametric formulation (Castro et al., 1990) solving the over-determined linear system of equations in a constrained least-squares sense. Details about the approach applied in central Italy are given by Bindi et al. (2018). Once the non-parametric source spectra are isolated from the other terms, we compute the seismic moment M_0 and the corner frequency (fc) from the best fitting omega-square source model (Brune, 1970), assuming an average S-wave radiation pattern $R^{\theta\phi}$=0.55, and average density and shear-wave velocity at the source equal to 2700 kg/m^3 and 3200 m/s, respectively. Finally, following Izutani and Kanamori (2001) and Venkataraman and Kanamori (2004), we assess the model-dependent radiated energy E_R from the integral of the squared velocity Brune source spectra (see also Picozzi et al., 2018, 2019a).

Regarding the strong motion features extracted from seismograms, following Picozzi et al. (2017 and 2019b), we consider the squared velocity signal integrated over the S-wave time window ($IV2_S$) and of S-wave peak-displacement (PD_S). The $IV2_S$ and PD_S values relevant to the *k*th earthquake recorded at the *i*th station are then linked to E_R and M_0, respectively, through the following empirical attenuation models:

$$log[IV2_S(R_H)]_{ki} = A + B \cdot log(E_R)_k + w_j C_j + \left(1 - w_j\right)C_{j+1} + \sum_{i=1}^{N_{sta}} \delta_{il} S_i \quad [1]$$

and

$$log[PD_S(R_H)]_{ki} = D + F \cdot log(M_0)_k + w_j G_j + \left(1 - w_j\right)G_{j+1} + \sum_{i=1}^{N_{sta}} \delta_{il} Z_i \quad [2]$$

where, the hypocentral distance (R_H) range is discretized into Nbin; the index j =1,..,Nbin indicates the *j*th node selected such that R_H is between the distances $r_j \leq R_H < r_j+1$; the attenuation function is linearized between nodes rj and rj+1 using the weights *w*, computed as $w_j = (r_j+1 - R_H)/(r_j+1 - rj)$. The distance range 2-150 km is discretized into 50 bins equally spaced on logarithmic scale. The S*i* and Z*i* terms are the station correction for station *i*, and N_{sta} is the number of stations. The coefficients *A*, *B*, C_j, *D*, *F*, and G_j are determined by solving the over-determined linear systems (Eqs. 1 and 2) in a least-square sense. To fix the trade-off between *A* and C_j, and as well *D* and G_j the attenuation is constrained to zero at r_2 equal to 5 km. The station corrections and the coefficients of the attenuation models are reported in Table S1 and S2, respectively (supplemental material). Positive station corrections are usually associated to high amplification effects as shown in Figure S1 (supplemental material) where two H/V are reported as examples. The calculated regressions have a R^2 equal to 0.93 and 0.92, respectively.

The observed $IV2_S$ and PD_S values corrected for the source scaling A+B log(E_R) and D+F log(M_0) are compared with the attenuation models C_j and G_j in Figures (7a) and (7b). The high number of events (i.e., ~6500) in the calibration data set, which corresponds to ~210.000 waveforms, made the attenuation models very robust. This is also indicated by the good agreement of the scaling with distance between model parameters and corrected data. Figures (7c) and (7d) show the comparison between the values E_R and M_0 computed by the spectral decomposition with the values obtained correcting $IV2_S$ and PD_S for attenuation effects as modeled through the C_j and $G_j$coefficients. These results suggest that the scaling coefficients A, B and D, F capture well the trend in the data over the entire energy and moment ranges. The station corrections Si and Zi are shown in Figures (7e and 7f), where the different branches correspond to different station channels.

Following the original idea of Kanamori et al. (1993), the E_R estimates are then used also to derive an energy-based local magnitude scale which agrees with ML_{IT16}. The advantage of calibrating a local magnitude scale on radiated energy (ML_{ER}) is that it can be extended toward larger magnitudes without saturation (i.e., differently from the classic ML scales based on the recordings deconvolution for the Wood-Anderson seismograms, ML_{ER} is not saturating). The best fit model obtained fitting ML_{IT16} as function of Log(E_R) is given by:

$$ML_{ER} = 0.56\ \mathrm{Log}(E_R) - 1.80 \qquad [3]$$

with standard deviation of the residuals equal to 0.09 magnitude units. We indicate with ML_{ER} the local magnitude obtained by applying equation (3).

RAMONES capabilities

To validate the capabilities of RAMONES, we apply the attenuation models of equations (1) and (2) to a dataset of events occurred in central Italy during 2019. These earthquakes were considered when performing the GIT inversion but were not considered for the calibration of attenuation models. This dataset is composed by 60 earthquakes with magnitude ML_{IT16} between 2.3 and 4.7 (Figure 1a). Figure (8a and 8b) compare the GIT estimates of E_R and M_0 with those retrieved with the RAMONES procedure. A good agreement among spectral estimates and those derived from waveforms analysis is observed over the whole explored range of seismic moment and energy. The $\mathrm{Log}(M_0)_{GIT}$-$\mathrm{Log}(M_0)_{RAMONES}$ residual distribution has mean and standard deviation values equal to $1.45 \cdot 10^{-4}$ and 0.2, respectively; the mean and standard deviation for the energy residuals are $6 \cdot 10^{-3}$ and 0.29, respectively. Since equations (1) and (2) are applied to each single recording, it is possible to compare the distribution of the single station RAMONES estimates of E_R and M_0 with the source parameters

obtained through the GIT inversion. The residuals between the GIT and RAMONES M_0 and E_R estimates for single recording do not show any particular trend neither with hypocentral distance and depth (Fig. 8c-f), nor with magnitude (Fig.8g-h). We observe a larger dispersion for seismic energy estimates (residuals standard deviation for E_R and M_0 is 0.29 and 0.2, respectively), but this agrees with the larger variability of this parameter observed during the model calibration.

Between January and September 2020, RAMONES computed the source parameters of about 800 earthquakes occurred in central and southern Apennines, Italy (Figure S21). Figure (9) shows the scaling of the seismic Energy E_R with moment M_0. Gray squares indicate data produced by the Ramones service in the period 1-1-2020 - September 2009, and black dots the calibration data set (2008-2018). During the 2020 testing phase, the RAMONES procedure is applied also to stations not considered during the calibration phase. Site specific adjustments in equations (1) and (2) for these stations are set to zero and they can be determined once enough local earthquakes have been recorded in the magnitude and distance ranges of interest. Similar to the procedure suggested to determine the local magnitude adjustments of new broadband or strong-motion stations installed in California (Uhrhammer et al., 2001), the statistical analysis of the residual distribution can provide robust estimates of the median corrections and their uncertainties.

Future perspectives

For testing its performances and for evaluating its potentiality, RAMONES is running since January 2020 with a configuration set to daily updates (Figure S2). For its long-term operability, several changes and developments in the operational configuration are possible. For rapid response actions, RAMONES can provide input information about source parameters that can be exploited, for example, for generating shaking maps more informative about the shaking potential of the earthquake and not based only on static information of the earthquake size given by the seismic moment (Di Giacomo and Bormann, 2011). The high potential of RAMONES is in its ability to provide timely information on the temporal evolution of static and dynamic source parameters. This could be particularly useful during a seismic sequence, as a change in the source dynamics provides information on the mechanics of earthquake ruptures. Therefore, for rapid response applications, the RAMONES computations can be switched to a modality triggered by alerting messages such as those issued by European–Mediterranean Seismological Centre. Other lines of development for RAMONES regard data accessibility and the extension of the monitored region. Regarding the modalities to retrieve data from RAMONES, future effort will be dedicated to make operative representational state transfer (RESTful) web services, preserving as much as possible the

compatibility with FDSN standards for event, station and data-select queries, and developing ad-hoc dictionaries when needed. As positive impact, the accessibility through web services will make possible the inter-operability of RAMONES with several other seismological services operating in Europe. To extend the applicability of RAMONES to other regions, new attenuation models for estimating E_R and M_0 from PD_S and $IV2_S$ have be developed, following the example of the harmonized local magnitude for Europe (Bindi et al., 2019). In conclusion, RAMONES represents, in our opinion, a fine example of how the open data policy pursued by the European seismological community since the last decade stimulated the grow of applications and services, which on the long term can have significant impact on mitigating seismic risk.

Data and Resources

We used data and information retrieved from EIDA (https://www.orfeus-eu.org/data/eida/), IRIS (https://www.iris.edu/hq/) and DPC (http://ran.protezionecivile.it/EN/index.php). The INGV bulletin is used to guide the data download (webservices.rm.ingv.it/fdsnws/event/1/) and to extract the earthquake locations. The International Federation of Digital Seismograph Networks (FDSN) specifications are available at http://www.fdsn.org/ and the Standard for the Exchange of Earthquake Data (SEED) manual is available at http://www.fdsn.org/pdf/SEEDManual_V2.4.pdf. For the calibration of the attenuation models, we used data mainly from networks IV (DOI: 10.13127/SD/X0FXnH7QfY), IT (DOI: 10.7914/SN/IT) and MN (DOI: 10.13127/SD/fBBBtDtd6q). In the application phase, we also processed data from networks GU (DOI: 10.7914/SN/GU), OT (DOI: 10.7914/SN/OT) and IX. The map in Figure 1 was prepared with the Generic Mapping Tools software package (http://gmt.soest.hawaii.edu/); R (R Core Team, 2018) and MATLAB R2019b (https://www.mathworks.com/products/matlab.html) were used for the regression analysis and for preparing the figures. The RAMONES service is reachable at: http://www.distav.unige.it/rsni/ramones.php

Acknowledgments

We thank M. Cattaneo for useful discussions and suggestions that we used for developing the service. Our gratitude is going also to both all network operators for sharing their data, and to EIDA and IRIS for maintaining their services.

355 **References**

356 Ameri, G., M. Massa, D. Bindi, E. D'Alema, A. Gorini, L. Luzi, M. Marzorati, F. Pacor, R. Paolucci,
357 R. Puglia, et al. (2009). The 6 April 2009 M w 6.3 L'Aquila (central Italy) earthquake: Strong-motion
358 observations, Seismol. Res. Lett. 80, 951–966

359 Andrews, D. J. (1986). Objective determination of source parameters and similarity of earthquakes
360 of different size, in Earthquake Source Mechanics, S. Das, J. Boatwright, and C. H. Scholz (Editors),
361 American Geophysical Union, Washington, pp. 259–267.

362 Bergamaschi F., Cultrera, G., Luzi, L., Azzara R. M., Ameri, G., Augliera P., Bordoni P., Cara F.,
363 Cogliano R., D'Alema, E., Di Giacomo, D., Di Giulio, G., Fodarella, A., Franceschina, G., Galadini,
364 F., Gallipoli, M. R., Gori, S., Harabaglia, P., Ladina, C., Lovati, S., Marzorati, S., Massa, M., Milana,
365 G., Mucciarelli, M., Pacor, F., Parolai, S., Picozzi, M., Pilz, M., Pucillo, S., Puglia R., Riccio, G. and
366 M. Sobiesiak, 2011. Evaluation of site effects in the Aterno river valley (Central Italy) from
367 aftershocks of the 2009 L'Aquila earthquake, Bull. Earthq. Eng., 9, 697–715.

368 Bindi, D., D. Spallarossa, M. Picozzi, D. Scafidi, and F. Cotton (2018). Impact of magnitude selection
369 on Aleatory variability associated with ground-motion prediction equations: Part I—Local, energy,
370 and moment magnitude calibration and stress-drop variability in Central Italy, Bull. Seismol. Soc.
371 Am. 108, no. 3A, 1427–1442, doi: 10.1785/0120170356.

372 Bindi D., R. Zaccarelli, A. Strollo, and D. Di Giacomo (2019). Harmonized local magnitude
373 attenuation function for Europe using the European Integrated Data Archive (EIDA). Geophys J Int
374 218(1):519–533

375 Bindi, D., D. Spallarossa, M. Picozzi, and P. Morasca (2020). Reliability of Source Parameters for
376 Small Events in Central Italy: Insights from Spectral Decomposition Analysis Applied to Both
377 Synthetic and Real Data, Bull. Seismol. Soc. Am., 1-19, doi: 10.1785/0120200126

378 Brune, J. N. (1970). Tectonic stress and the spectra of shear waves from earthquakes, J. Geophys.
379 Res. 75, 4997–5009.

380 Cara F., Cultrera G., Riccio G., Amoroso S., Bordoni P., Bucci A., D'Alema E., D'Amico M., Cantore
381 L., Carannante S., Cogliano R., Di Giulio G., Di Naccio D., Famiani D., Felicetta C., Fodarella A.,
382 Franceschina G., Lanzano G., Lovati S., Luzi L., Mascandola C., Massa M., Mercuri A., Milana G.,
383 Pacor F., Piccarreda D., Pischiutta M., Pucillo S., Puglia R., Vassallo M., Boniolo G., Caielli G.,
384 Corsi A., de Franco R., Tento A., Bongiovanni G., Hailemikael S., Martini M., Paciello A., Peloso

385 A., Verrubbi V., Gallipoli MR., Stabile T.A., Mancini M. (2019), Temporary dense seismic network
386 during the 2016 Central Italy seismic emergency for microzonation studies. Sci Data6, 182 (2019).
387 https://doi.org/10.1038/s41597-019-0188-1

388 Castro, R. R., J. G. Anderson, and S. K. Singh (1990). Site response, attenuation and source spectra
389 of S waves along the Guerrero, Mexico, subduction zone, Bull. Seismol. Soc. Am. 80, 1481–1503.

390 Chiaraluce, L., R. Di Stefano, E. Tinti, L. Scognamiglio, M. Michele, E. Casarotti, M. Cattaneo, P.
391 De Gori, C. Chiarabba, G. Monachesi, et al. (2017). The 2016 Central Italy seismic sequence: A first
392 look at the mainshocks, aftershocks, and source models, Seismol. Res. Lett. 88, doi:
393 10.1785/0220160221.

394 Cultrera *G.*, D'Alema *E.*, Amoroso *S.*, Angioni *B.*, Bordoni *P.*, Cantore *L.*, Cara *F.*, Caserta *A.*,
395 Cogliano *R.*, D'Amico *M.*, Di Giulio *G.*, Di Naccio *D.*, Famiani *D.*, Felicetta *C.*, Fodarella *A.*, Lovati
396 *S.*, Luzi *L.*, Massa *M.*, Mercuri *A.*, Milana *G.*, Pacor *F.*, Pischiutta *M.*, Pucillo *S.*, Puglia *R.*, Riccio *G.*,
397 Tarabusi *G.*, Vassallo *M. and* C. Mascandola, 2016, Site effect studies following the 2016 Mw 6.0
398 Amatrice earthquake (Italy): the Emersito Task Force activities, Annals of Geophysics 59,
399 doi.org/10.4401/ag-7189

400 Di Bona, M. (2016). A local magnitude scale for crustal earthquakes in Italy, Bull. Seismol. Soc. Am.
401 106, 242–258.

402 Di Giacomo, D. and P. Bormann (2011). The moment magnitude Mw and the energy magnitude Me:
403 common roots and differences, J. Seismol., 15, 411–427.

404 Hanks T. C., Kanamori H., 1979. A moment magnitude scale, J. Geophys. Res., 84, 2348–2350,
405 doi:10.1029/JB084iB05p02348.

406 Kanamori, H., E. Hauksson, L. K. Hutton, and L. M. Jones (1993). Determination of earthquake
407 energy release and M L using TERRAscope, Bull. Seismol. Soc. Am. 83, 330–346.

408 Kanamori, H. (2005), Real-time seismology and earthquake damage mitigation, Annu. Rev. Earth
409 Planet. Sci., 33, 195–214, doi:10.1146/annurev.earth.33.092203.122626.

410 Izutani, Y. and H. Kanamori, (2001). Scale-dependence of seismic energy-to-moment ratio for strike-
411 slip earthquakes in Japan, Geophys. Res. Lett., 28, 4007–4010.

412 Kanamori, H., E. Hauksson, L. K. Hutton, and L. M. Jones (1993). Determination of earthquake
413 energy release and M L using TERRAscope, Bull. Seismol. Soc. Am. 83, 330–346.

414 Kanamori, H. (2005), Real-time seismology and earthquake damage mitigation, Annu. Rev. Earth

Planet. Sci., 33, 195–214, doi:10.1146/annurev.earth.33.092203.122626.

Kong, Q., Trugman, D. T., Ross, Z. E., Bianco, M. J., Meade, B. J., and Gerstoft, P. (2019). Machine learning in seismology: Turning data into insights. Seismological Research Letters, 90(1), 3–14. https://doi.org/10.1785/0220180259

Lomax, A., J. Virieux, P. Volant, and C. Thierry-Berge (2000). Probabilistic earthquake location in 3D and layered models, in Advances in Seismic Event Location, C. H. Thurber and N. Rabinowitz (Editors), Kluwer Academic Publishers, Dordrecht/Boston/London, 101–134.

Margheriti, L., Chiaraluce, L., Voisin, C., Cultrera, G., Govoni, A., Moretti, M., Bordoni, P., Luzi, L., Azzara, R., Valoroso, L., Di Stefano, R., Mariscal, A., Improta, L., Pacor, F., Milana, G, Mucciarelli, M., Parolai, S., Amato, A., Chiarabba, C., De Gori, P., Lucente, F.P., Di Bona, M., Pignone, M., Cecere, G., Criscuoli, F., Delladio, A., Lauciani, V., Mazza, S., Di Giulio, G., Cara, F., Augliera, P., Massa, M., D'Alema, E., Marzorati, S., Sobiesiak, M., Strollo, A., Duval, A-M., Dominique, P., Delouis, B., Paul, A., Husen, S. and G. Selvaggi, 2011. Rapid response seismic networks in Europe: lessons learnt from the L'Aquila earthquake emergency, Ann. Geophys., 54, (4), 392–399.

Mousavi, S. M., Zhu, W., Sheng, Y., and Beroza, G. C. (2019a). CRED: A deep residual network of convolutional and recurrent units for earthquake signal detection. Scientific Reports, 9(1), 10,267

Mousavi, S. M., Zhu, W., Ellsworth, W., & Beroza, G. (2019b). Unsupervised Clustering of Seismic Signals Using Deep Convolutional Autoencoders. IEEE Geoscience and Remote Sensing Letters, 16(11), 1693–1697. https://doi.org/10.1109/LGRS.2019.2909218

Münchmeyer, J., Bindi, D., Sippl, C., Leser, U., and Tilmann, F. (2019). Low uncertainty multifeature magnitude estimation with 3-D corrections and boosting tree regression: application to North Chile. Geophysical Journal International, 220(1), 142-159

Nolet, G., B. Romanovicz, R. Kind and E. Wielandt (1986). The ORFEUS science plan, 45 pp., D. Reidel Publishing Co., Dordrecht

Oth, A., D. Bindi, S. Parolai, and D. Di Giacomo (2011). Spectral analysis of K-NET and KiK-net data in Japan. Part II: On attenuation characteristics, source spectra, and site response of borehole and surface stations, Bull. Seismol. Soc. Am. 101, 667–687.

Pacor, F., D. Spallarossa, A. Oth, L. Luzi, R. Puglia, L. Cantore, A. Mercuri, M. D'Amico, and D. Bindi (2016). Spectral models for ground motion prediction in the L'Aquila region (central Italy):

445 Evidence for stress-drop dependence on magnitude and depth, Geophys. J. Int. 204, 697–718.

446 Picozzi, M., D. Bindi, P. Brondi, D. Di Giacomo, S. Parolai, and A. Zollo (2017). Rapid determination
447 of P wave- based energy magnitude: insights on source parameter scaling of the 2016 Central Italy
448 earthquake sequence, Geophys. Res. Lett., 44, 4036–4045.

449 Picozzi, M., Bindi, D., Spallarossa, D., Di Giacomo, D. and A. Zollo (2018). A rapid response
450 magnitude scale for timely assessment of the high frequency seismic radiation, Scientific Reports –
451 Nature, 8, 8562, https://doi.org/10.1038/s41598-018-26938-9.

452 Picozzi, M., Bindi, D., Spallarossa, D., Oth, A., Di Giacomo, A. and A Zollo et al. (2019a). Moment
453 and energy magnitudes: diversity of views on earthquake shaking potential and earthquake statistics.
454 Geophys. J. Int. 216, 1245-1259, doi: 10.1093/gji/ggy488.

455 Picozzi, M., Bindi, D., Zollo, A. et al. Detecting long-lasting transients of earthquake activity on a
456 fault system by monitoring apparent stress, ground motion and clustering. Sci Rep 9, 16268 (2019b).
457 doi:10.1038/s41598-019-52756-8

458 R Core Team (2018). R: A language and environment for statistical computing, R Foundation for
459 Statistical Computing, Vienna, Austria, available at https://www.r-project.org/ (last accessed June
460 2018).

461 Ross, Z. E., Hauksson, E., and Y. Ben-Zion (2017). Abundant off-fault seismicity and orthogonal
462 structures in the San Jacinto fault zone. Science Advances Vol. 3, no. 3, e1601946. DOI:
463 10.1126/sciadv.1601946

464 Ross, Z. E., Trugman, D. T., Hauksson, E., and Shearer, P. M. (2019). Searching for hidden
465 earthquakes in Southern California. Science, 364(6442), 767–771.
466 https://doi.org/10.1126/science.aaw6888

467 Scafidi, D., D. Spallarossa, C. Turino, G. Ferretti, and A. Viganò (2016). Automatic P- and S-wave
468 local earthquake tomography: Testing performance of the automatic phase-picker engine RSNI-
469 Picker, Bull. Seismol. Soc. Am. 106, no. 2, 526–536, doi: 10.1785/0120150084.

470 Scafidi, D., D. Spallarossa, G. Ferretti, S. Barani, B. Castello and L. Margheriti (2019). A Complete
471 Automatic Procedure to Compile Reliable Seismic Catalogs and Travel-Time and Strong-Motion
472 Parameters Datasets Seism. Rese. Letters 90 (3): 1308-1317. https://doi.org/10.1785/0220180257

473 Spallarossa, D., D. Bindi, P. Augliera, and M. Cattaneo (2002). An ML scale in northwestern Italy,
474 Bull. Seismol. Soc. Am. 92, 2205–2216.

Spallarossa, D., G. Ferretti, D. Scafidi, C. Turino, and M. Pasta (2016). Performance of the RSNI-Picker, Seismol. Res. Lett. 85, 1243–1254.

Spallarossa, D., M. Cattaneo, D. Scafidi, M. Michele, L. Chiaraluce, M. Segou, and I. Main (2020). An automatically generated high-resolution seismic catalogue for the 2016-2017 Central Italy sequence, including P and S phase arrival times, submitted to Geophys. J. Int.

Uhrhammer, R. A., M. Hellweg, K. Hutton, P. Lombard, A. W. Walters, E. Hauksson and D. Oppenheimer (2011). California Integrated Seismic Network (CISN) local magnitude determination in California and vicinity, \Bull. Seism. Soc. Am., 101, 2685-2693.

Venkataraman, A. and H. Kanamori (2004). Observational constraints on the fracture energy of subduction zone earthquakes, J. geophys. Res., 109, B05302, doi:10.1029/2003JB002549.

Wyss, M., and J. N. Brune (1968). Seismic moment, stress, and source dimensions for earthquakes in the California–Nevada region, J. Geophys. Res. 73, 4681–4694.

Zhang, M., W. L. Ellsworth and G. C. Beroza (2019). Rapid Earthquake Association and location Seism. Res. Letters (2019) 90 (6): 2276-2284. https://doi.org/10.1785/0220190052

Zhu, W., and Beroza, G. C. (2018). PhaseNet: A deep-neural-network-based seismic arrival time picking method. Geophysical Journal International, 216(1), 261–273.

Full mailing address for each author

Daniele Spallarossa

Dipartimento di Scienze della Terra dell'Ambiente e della Vita (DISTAV),
University of Genoa, Viale Benedetto XV 5, 16132 Genoa, Italy
daniele.spallarossa@unige.it

Matteo Picozzi

University of Naples Federico II, Department of Physics
via Cinthia 21, 80126 Naples, Italy
matteo.picozzi@unina.it

Davide Scafidi

Dipartimento di Scienze della Terra dell'Ambiente e della Vita (DISTAV),
University of Genoa, Viale Benedetto XV 5, 16132 Genoa, Italy
davide.scafidi@unige.it

Paola Morasca

Istituto Nazionale di Geofisica e Vulcanologia INGV,
via A. Corti 12, 20133 Milan, Italy
paola.morasca@ingv.it

Chiara Turino

Dipartimento di Scienze della Terra dell'Ambiente e della Vita (DISTAV),
University of Genoa, Viale Benedetto XV 5, 16132 Genoa, Italy
chiara.turino@edu.unige.it

Dino Bindi

German Research Centre for Geoscience GFZ,
Telegrafenberg, 14473 Potsdam, Germany
bindi@gfz-potsdam.de

Figure captions

Figure 1. Screenshot of the webpage relevant to the application of RAMONES in central Italy. A map with locations and a table with source parameters are shown for earthquakes analyzed since January 2020. Within the table, a link to a specific event page (Figure 2) is provided. Using the "Seismic stations" selections, a map of the station locations and relevant metadata is shown. Different scaling relationships are shown in Figures refreshed following the RAMONES updates. See text for more details.

Figure 2. Screenshot of the RAMONES event-specific webpage. The epicentral location of the earthquakes (circle) and the station locations (triangles) are shown in a map, whereas the source parameters and station specific estimates of different ground motion features (e.g. the peak ground acceleration PGA and peak ground velocity PGV for the three components) are listed in two different tables. Station specific estimates of seismic moment (M_0) and radiated energy (E_R) are listed as well. See text for more details.

Figure 3. Map showing the earthquake locations (circles) and the station locations (triangles) relevant to the data set used for calibrating and validating the attenuation models implemented by RAMONES.

Figure 4. Data set used for calibrating the models used by RAMONES for estimating M_0 and E_R. a) Local magnitude versus hypocentral distance distribution of the considered recordings; b) Distributions of the hypocentral depths. c) Number of recordings used for the HH (broad band), EH (short period) and HN (accelerometers) channels. d) Empirical cumulative distribution of the number of recording per station and per event.

Figure 5. RAMONES workflow for deriving and applying the empirical models relating the ground motion features PD_S (i.e., peak displacement over S-waves) and $IV2_S$ (i.e., integral of the squared velocity over the S-wave window) to the estimates of seismic moment (M_0) and radiated energy (E_R). In the workflow, retrospective analysis indicates the operations performed for calibrating the empirical models starting from the source parameters provided by the spectral decomposition; prospective analysis indicates the application of the models to new data (operational phase).

Figure 6. Distribution with hypocentral distance of the peak displace over the S-wave window (panel a) and of the integral of the squared velocity over the S-wave window (panel b). The trends of the parameters averaged over three narrow magnitude ranges as indicated in the panels (white line and gray ribbon) are also shown.

Figure 7. Results of the calibrations between $IV2_S$ and E_R (Eq.1) and between PD_S and M_0 (Eq.2). a) the coefficients G_j in Eq.2 (white stars) +/- 1 standard deviation (grey area) are compared with the residuals $\Delta log(M_0) = log[PD_S(R_H)] - D + Flog(M_0)$ (black dots). b) The same as a), but for the coefficients C_j of Eq.1 (white stars) that are compared with the residuals $\Delta log(E_R) = log[IV2_S(R_H)] - A - Blog(E_R)$ (black dots). c) PD_S values corrected for G_j are compared with $M_{0(obs)}$ (the corrected values for each recording are in black, the average for each earthquake is plot as white star). d) The same as c), but $IV2_S$ values corrected for C_j are compared with the energy $E_{R(obs)}$. e) Station correction coefficients Z_i (Eq.2). f) The same as e), but for station correction coefficients S_i (Eq.1). Station corrections are reported in Table 1S (supplementary material)**.**

Figure 8. Comparison of E_R and M_0 estimates obtained from GIT and RAMONES for 2019 earthquakes data. a) log(M_0) from GIT vs. RAMONES; +/- 1 standard deviation for RAMONES estimates (colored vertical bars) and 1:1 scaling relation (black line). b) The same as a), but for log(E_R). c) Residuals between the GIT and RAMONES for log(M_0) estimates for single recording with hypocentral distance (dots colored per density of data); +/- 1 standard deviation (black dashed lines). d) The same as c), but for log(E_R) residuals. e) and f), the same as d) and c), respectively, but for magnitude. g) and h), the same as d) and c), respectively, but for hypocentral depth.

Figure 9. Scaling of the seismic energy E_R with moment M_0. Gray squares indicate the Ramones data set (from January 2020 to September 2009) and black dots are relevant to the calibration data set (2008-2018).

Figures

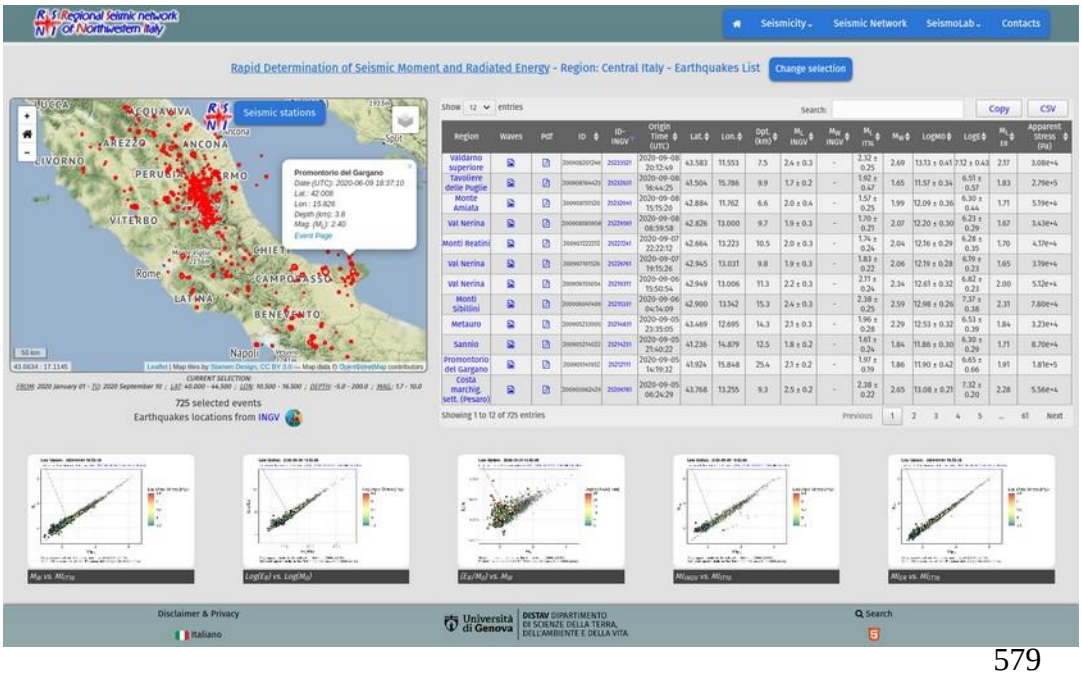

Figure 1. Screenshot of the webpage relevant to the application of RAMONES in central Italy. A map with locations and a table with source parameters are shown for earthquakes analyzed since January 2020. Within the table, a link to a specific event page (Figure 2) is provided. Using the "Seismic stations" selections, a map of the station locations and relevant metadata is shown. Different scaling relationships are shown in Figures refreshed following the RAMONES updates. See text for more details.

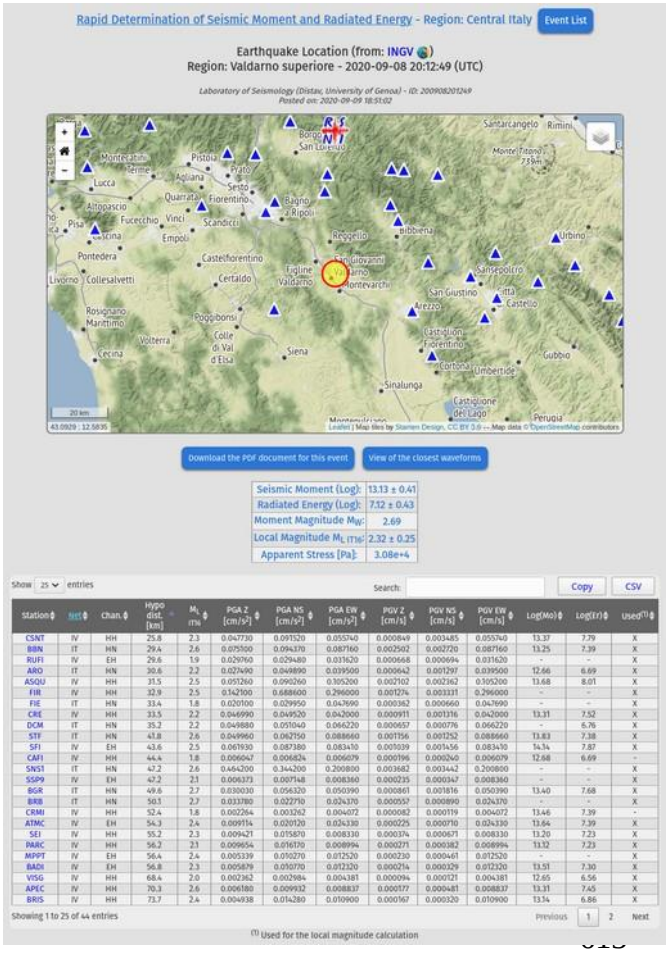

Figure 2. Screenshot of the RAMONES event-specific webpage. The epicentral location of the earthquake (circle) and the station locations (triangles) are shown in a map whereas the source parameters and station specific estimates of different ground motion features (e.g. the peak ground acceleration PGA and peak ground velocity PGV for the three components) are listed in two different tables. Station specific estimates of seismic moment (M_0) and radiated energy (E_R) are listed as well. See text for more details.

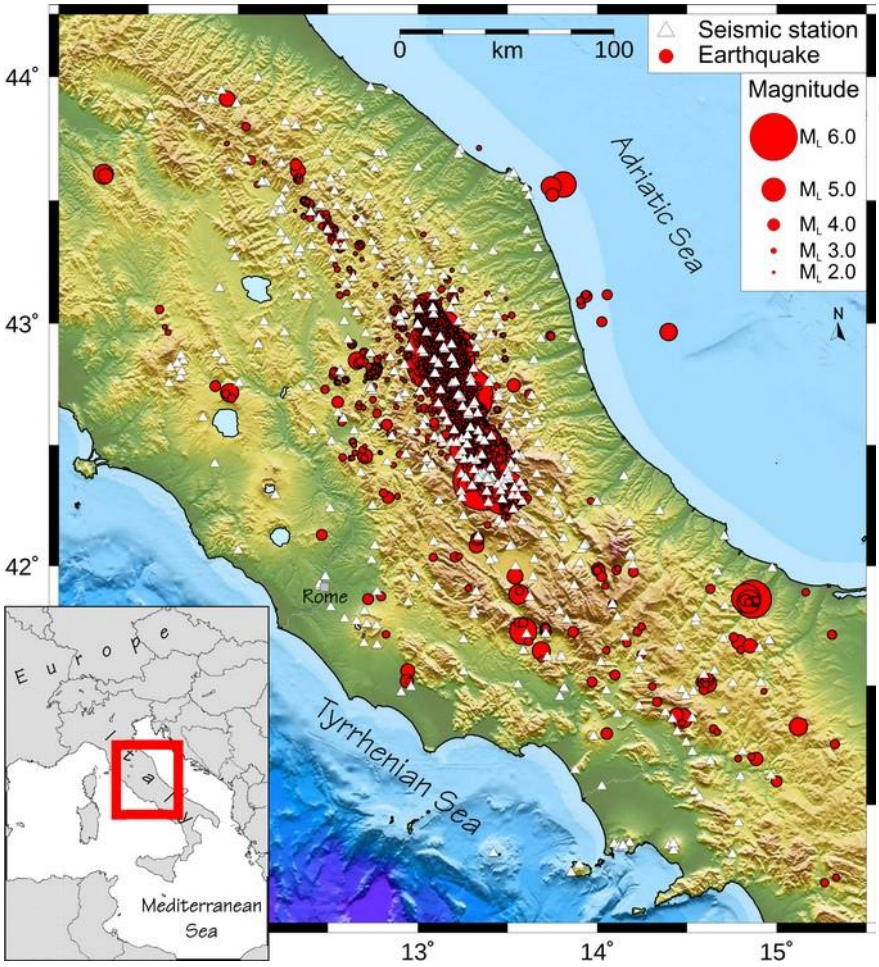

639

640 **Figure 3**. Map showing the earthquake locations (circles) and the station locations (triangles) relevant to the
641 data set used for calibrating and validating the attenuation models implemented by RAMONES.

642

643

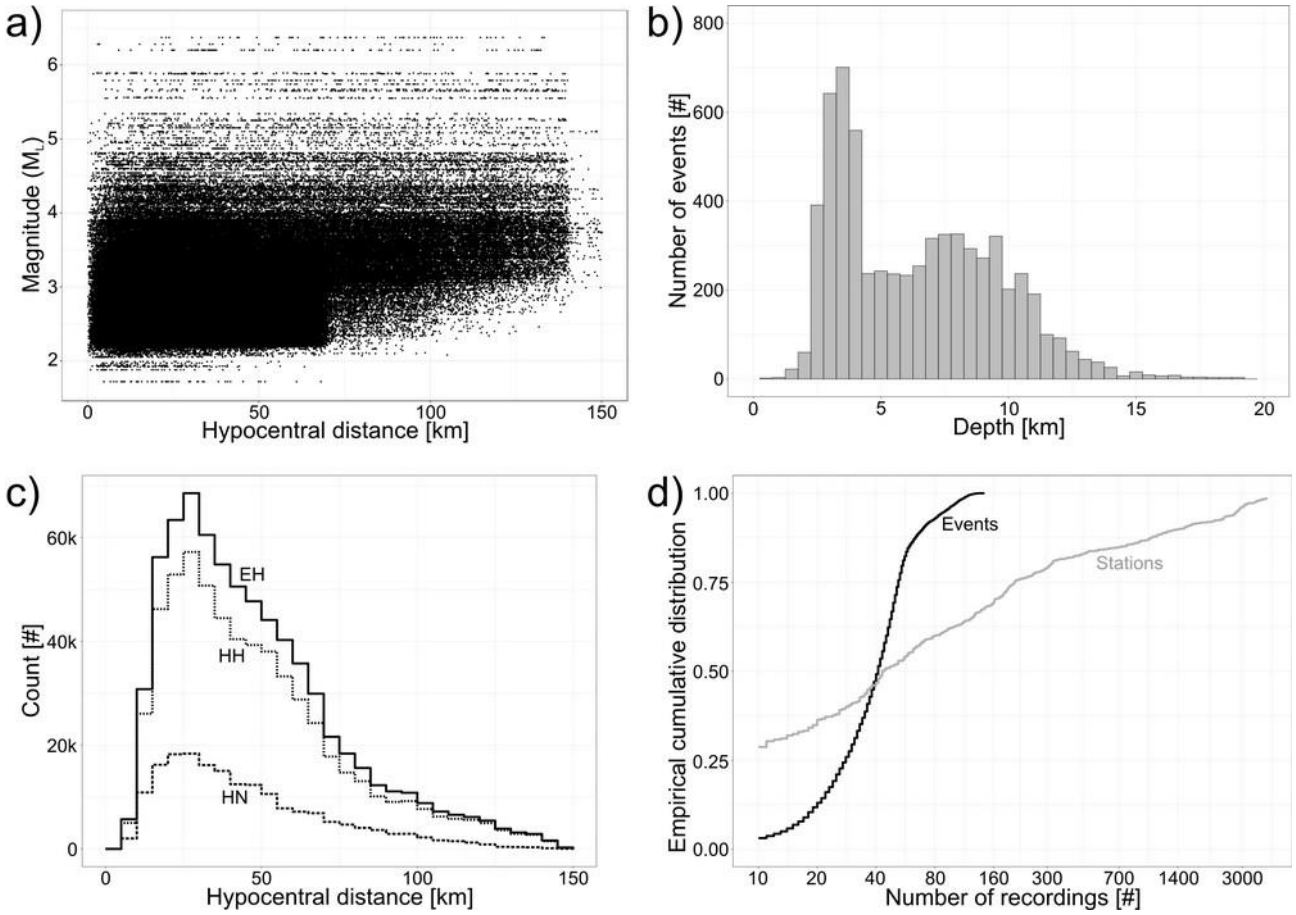

644

645 **Figure 4.** Data set used for calibrating the models used by RAMONES for estimating M_0 and E_R. a) Local
646 magnitude versus hypocentral distance distribution of the considered recordings; b) Distributions of the
647 hypocentral depths. c) Number of recordings used for the HH (broad band), EH (short period) and HN
648 (accelerometers) channels. d) Empirical cumulative distribution of the number of recording per station and per
649 event.

650

651

652

653

654

655

656

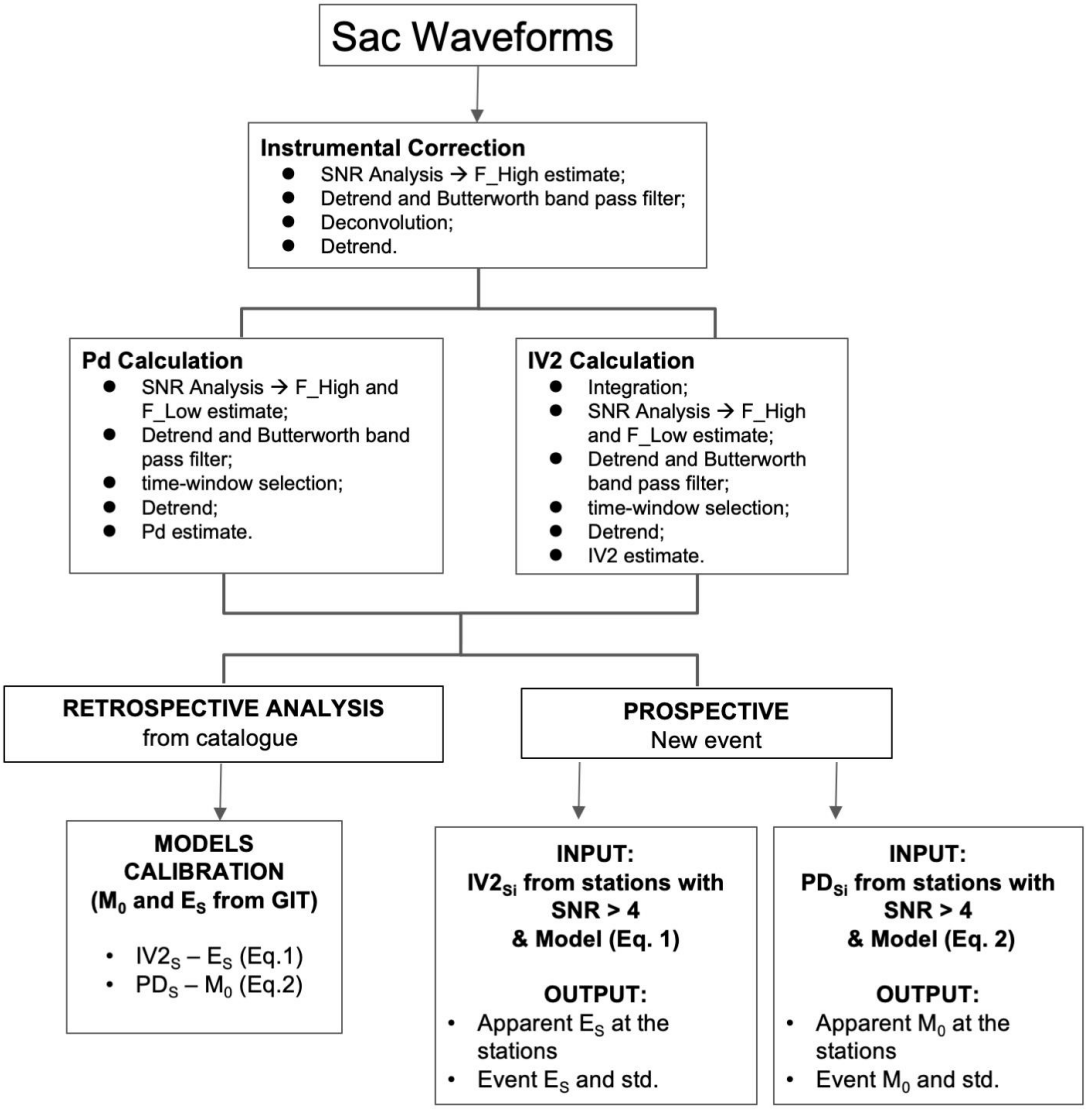

657 **Figure 5**. RAMONES workflow for deriving and applying the empirical models relating the ground motion
658 features PD_S (i.e., peak displacement over S-waves) and $IV2_S$ (i.e., integral of the squared velocity over the S-
659 wave window) to the estimates of seismic moment (M_0) and radiated energy (E_R). In the workflow,
660 retrospective analysis indicates the operations performed for calibrating the empirical models starting from the
661 source parameters provided by the spectral decomposition; prospective analysis indicates the application of
662 the models to new data (operational phase).

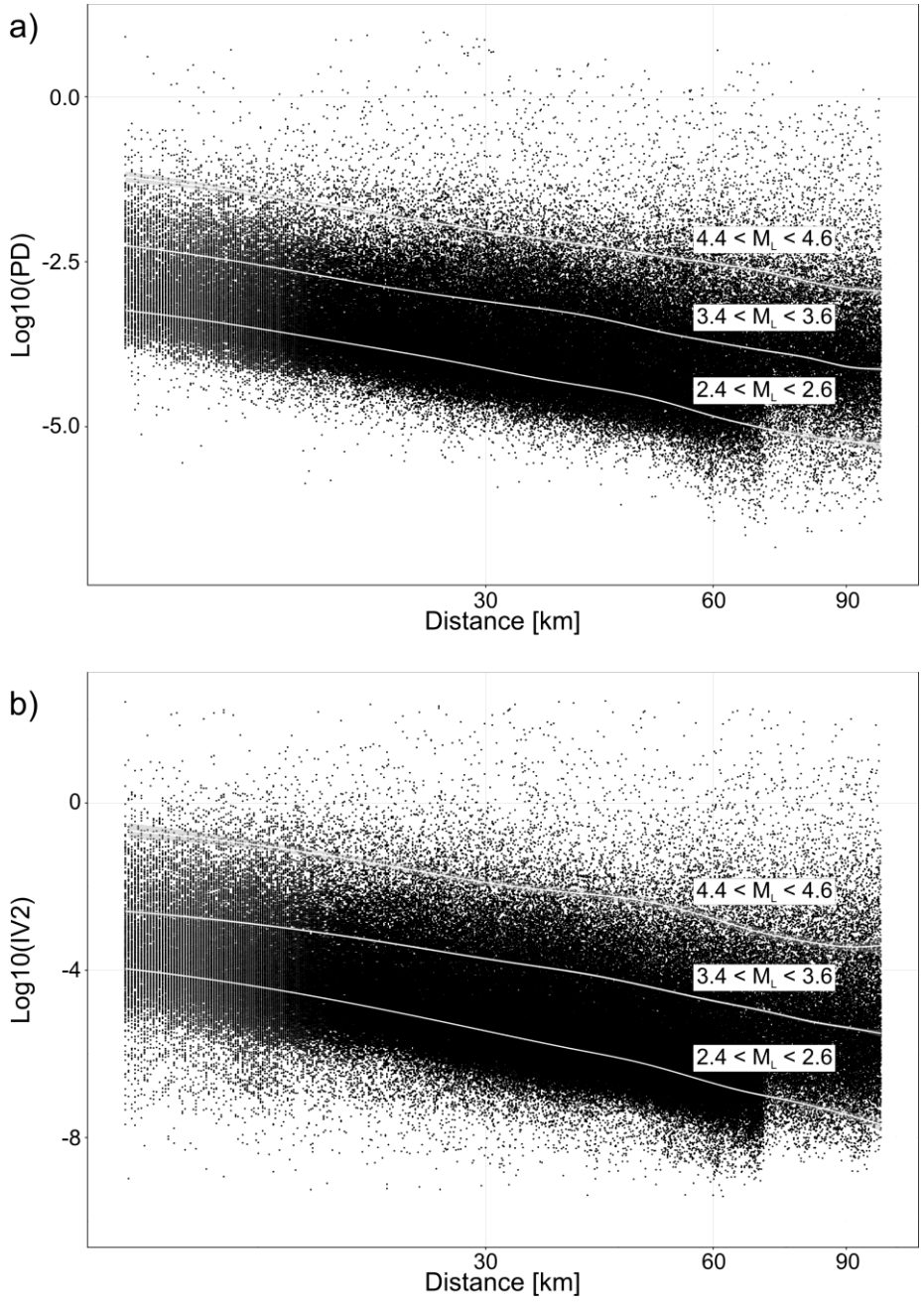

Figure 6. Distribution with hypocentral distance of the peak displace over the S-wave window (panel a) and of the integral of the squared velocity over the S-wave window (panel b). The trends of the parameters averaged over three narrow magnitude ranges as indicated in the panels (white line and gray ribbon) are also shown.

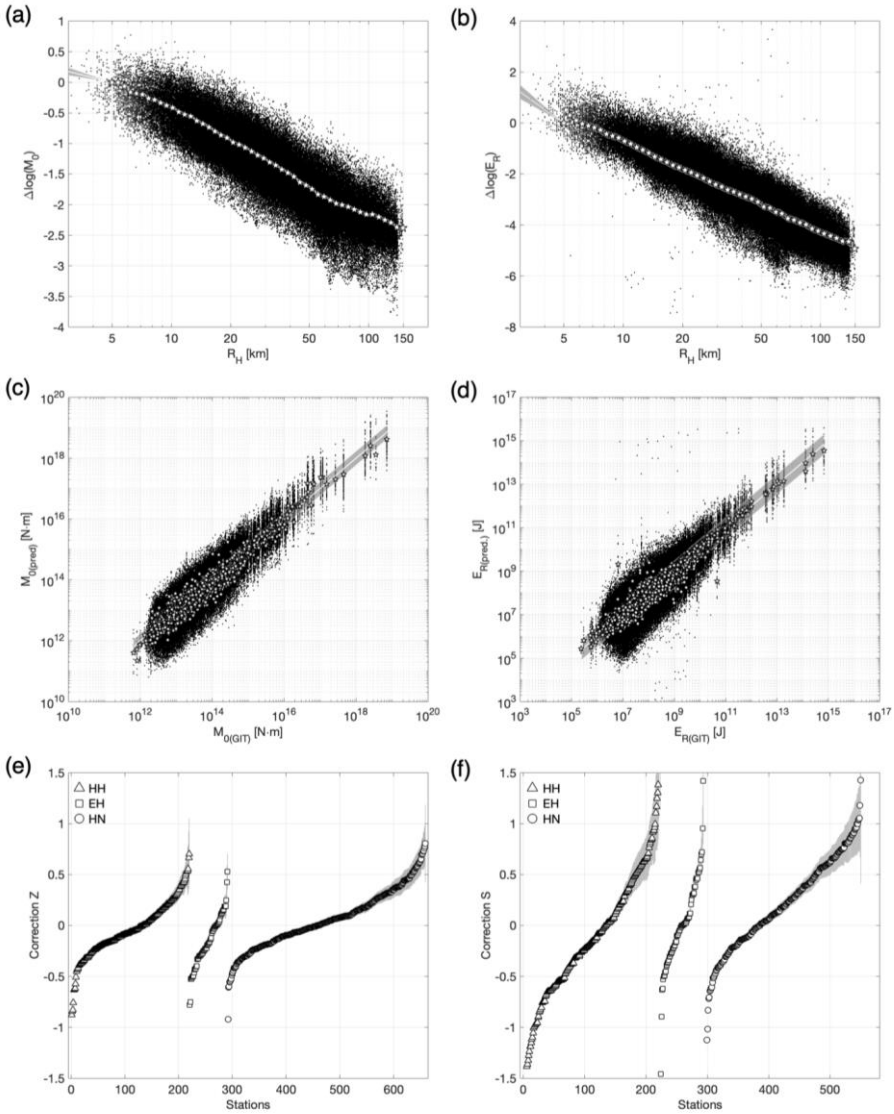

Figure 7. Results of the calibrations between $IV2_S$ and E_R (Eq.1) and between PD_S and M_0 (Eq.2). a) the coefficients G_j in Eq.2 (white stars) +/- 1 standard deviation (grey area) are compared with the residuals $\Delta log(M_0) = log[PD_S(R_H)] - D + Flog(M_0)$ (black dots). b) The same as a), but for the coefficients C_j of Eq.1 (white stars) that are compared with the residuals $\Delta log(E_R) = log[IV2_S(R_H)] - A - Blog(E_R)$ (black dots). c) PD_S values corrected for G_j are compared with $M_{0(obs)}$ (the corrected values for each recording are in black, the average for each earthquake is plot as white star). d) The same as c), but $IV2_S$ values corrected for C_j are compared with the energy $E_{R(obs)}$. e) Station correction coefficients Z_i (Eq.2). f) The same as e), but for station correction coefficients S_i (Eq.1). Station corrections are reported in Table 1S (supplementary material).

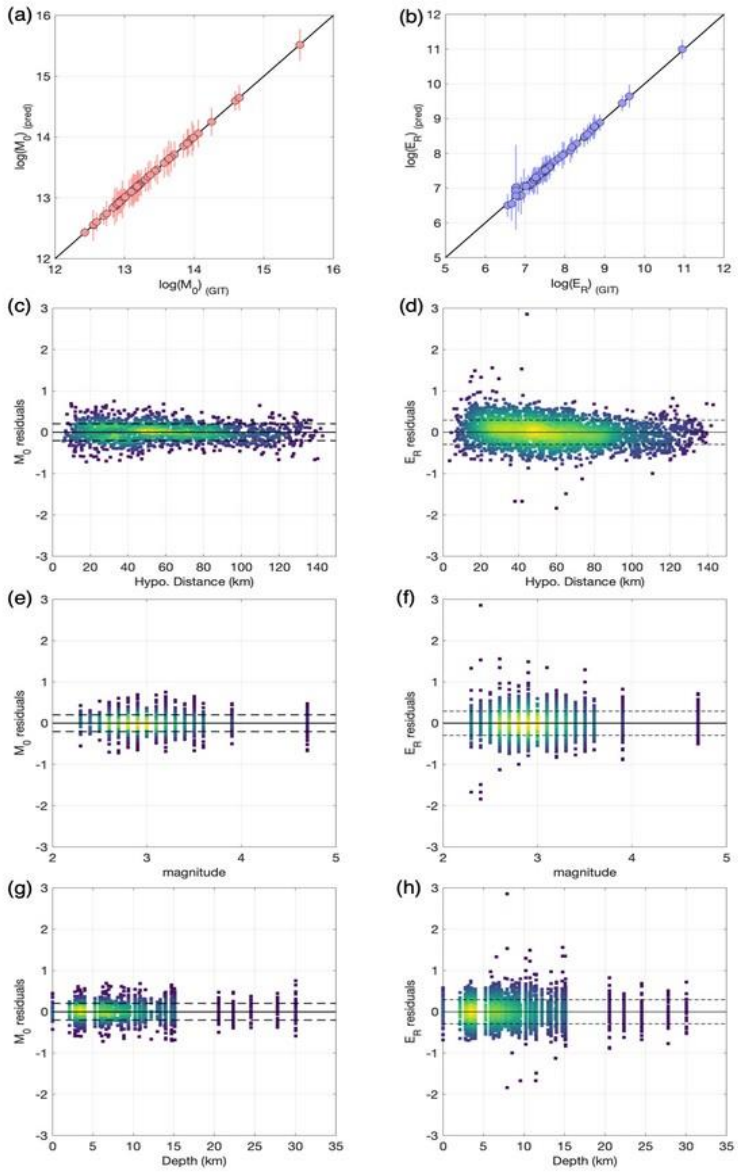

Figure 8. Comparison of E_R and M_0 estimates obtained from GIT and RAMONES for 2019 earthquakes data. a) log(M_0) from GIT vs. RAMONES; +/- 1 standard deviation for RAMONES estimates (colored vertical bars) and 1:1 scaling relation (black line). b) The same as a), but for log(E_R). c) Residuals between the GIT and RAMONES for log(M_0) estimates for single recording with hypocentral distance (dots colored per density of data); +/- 1 standard deviation (black dashed lines). d) The same as c), but for log(E_R) residuals. e) and f), the same as d) and c), respectively, but for magnitude. g) and h), the same as d) and c), respectively, but for hypocentral depth.

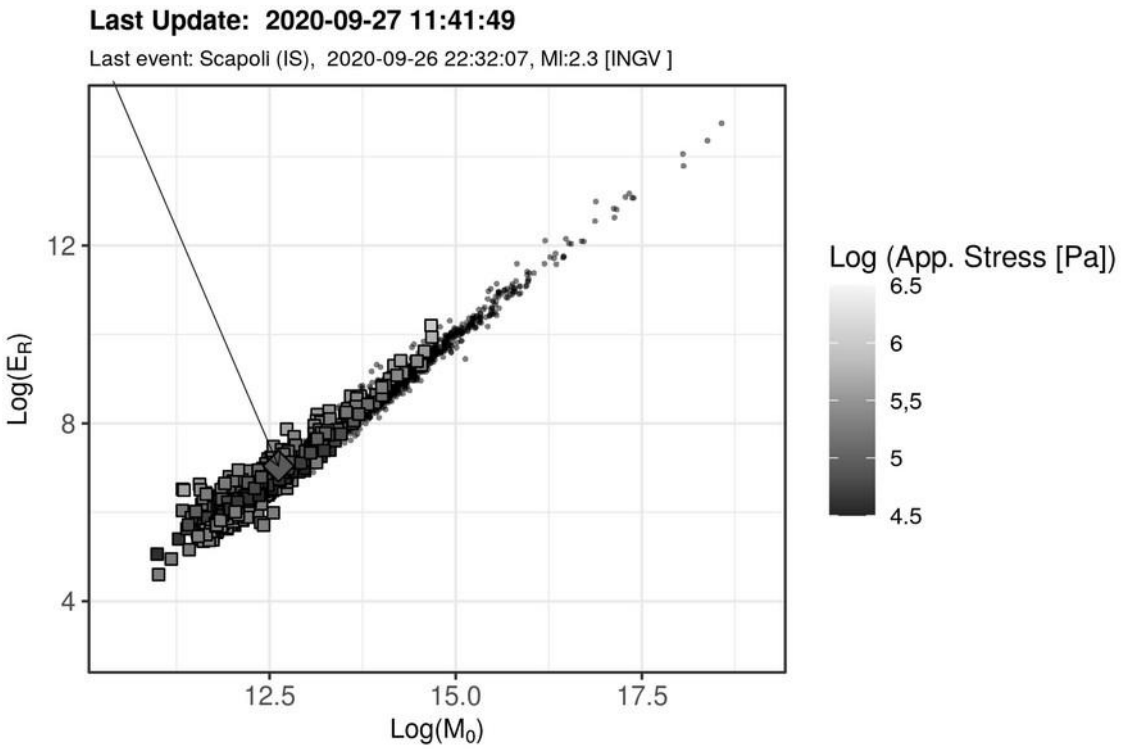

Figure 9. Scaling of the seismic energy E_R with moment M_0. Gray squares indicate the Ramones data set (from January 2020 to September 2009) and black dots are relevant to the calibration data set (2008-2018).

RAMONES, the Rapid Assessment of MOmeNt and Energy Service in Central Italy: Concepts, capabilities and future perspectives

Supplementary information

Daniele Spallarossa[1,2], Matteo Picozzi[3], Davide Scafidi[1], Paola Morasca[2], Chiara Turino and Dino Bindi[4]
[1]University of Genova, Italy
[2]INGV, Milano, Italy
[3]University of Naples Federico II, Italy
[4]Helmholtz Centre Potsdam, GFZ German Research Centre for Geosciences, Germany

Introduction

The Supplementary Information contains information about:

a) Figure S1

Figure S1 exemplifies the horizontal-to-vertical spectral ratio (H/V) for two stations (NRCA and PTQR). The H/V curves are computed considering both S-waves and noise windows, as indicated in the legend. The average ± one standard deviation of the ratios computed for several windows are shown. PTQR is an example of station free from significant site amplifications and a strong negative station corrections for $IV2_S$ is obtained (see Table S1 and equation 1 of the article); station NCRA shows strong amplifications between 5 and 10 Hz and the station correction for $IV2_S$ is large and positive.

b) Figure S2

Figure S2 shows the location of the events (red circles) automatically elaborates by the RAMONES between January and September 2020. The location of the stations providing the recordings analyzed by the service are shown with triangles. The rectangular area delimits the region used to extract the event information from the INGV catalog.

c) Table S1

Stations analyzed by RAMONES. The columns report:

Code: station name; lat: latitude of the station location; lon: longitude of the station location; Net: network of the station; S_HH, Z_HH: station corrections for channels HH relevant to equations 1 (S_HH, model for $IV2_S$) and 2 (Z_HH, model for PD_S); S_EH, Z_EH: station corrections for channels EH; S_HN, Z_HN: station corrections for channels HN

d) Table S2

Coefficients of the empirical models described by equations 1 and 2 of the article.

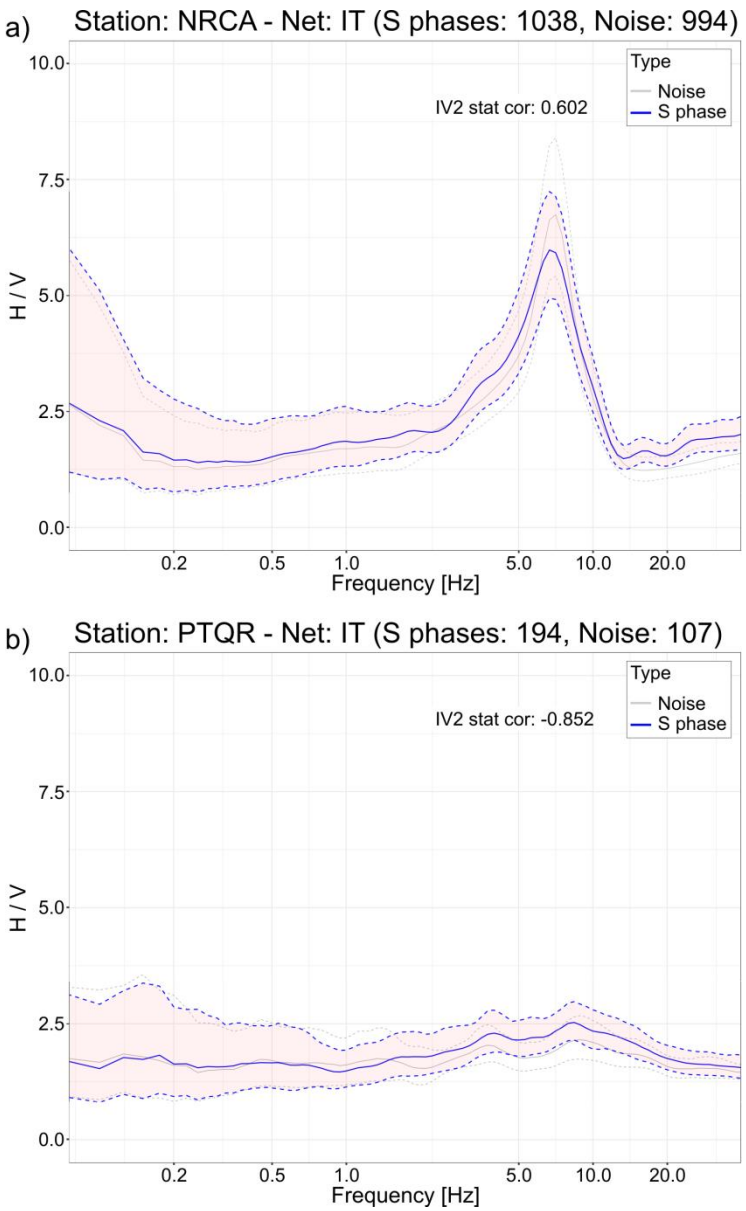

Figure S1: H/V curves for stations NRCA (a) and PTQR (b). Spectral ratios on ambient noise (dotted gray lines) and earthquake recordings (blue lines and pink shaded area), are computed on fixed time windows of 12s (pre-event and S-wave phase)

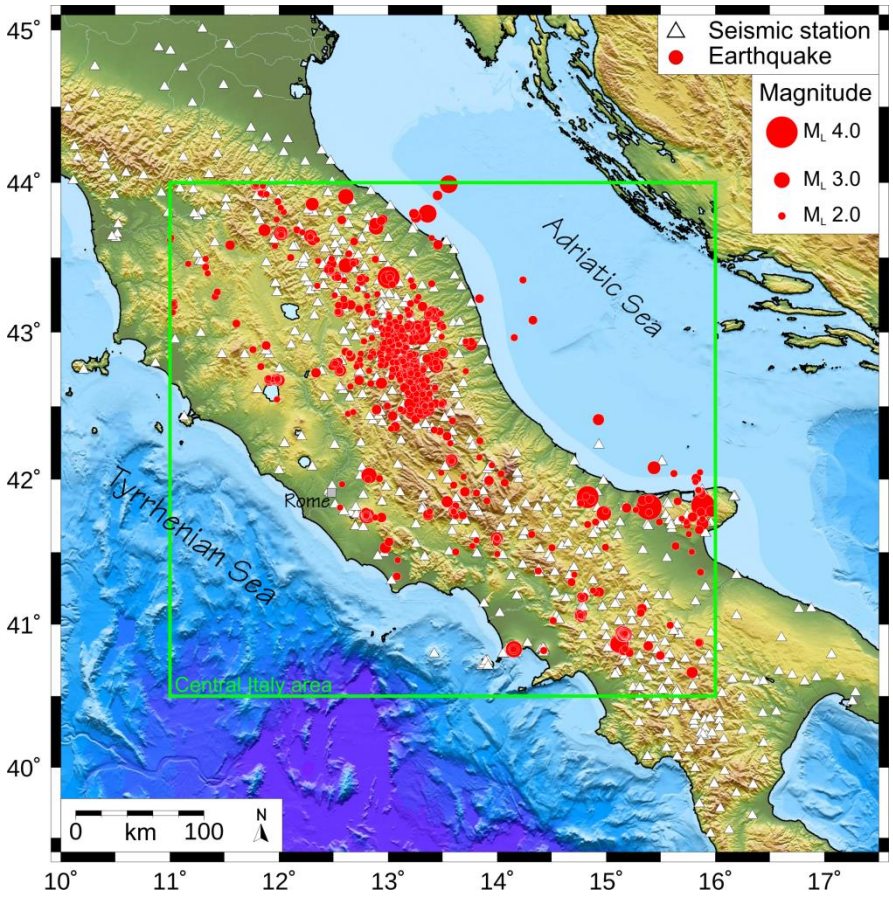

Figure S2: Map of the events (red circles) and stations (white triangles) automatically elaborates by the RAMONES service in the period from January to September 2020. The green polygon indicate the extent of the area used to extract the event information from the INGV catalog.

Code	Lat	Lon	Net	S_HH, Z_HH	S_EH, Z_EH	S_HN, Z_HN
0CAN	43.472	12.631	IT	- , -	- , -	0.046 , -0.248
0MBT	43.462	12.249	IT	- , -	- , -	- , 0.448
0PIO	43.587	12.513	IT	- , -	- , -	-0.515 , -0.407
0REN	43.546	12.264	IT	- , -	- , -	-0.832 , -0.471
0UM0	43.286	12.335	IT	- , -	- , -	- , -0.347
0UM8	43.304	12.341	IT	- , -	- , -	- , 0.419
ACC	42.696	13.242	IT	- , -	- , -	-0.105 , -0.001
ACER	40.787	15.943	IV	-0.449 , 0.200	- , -	- , -
ACT	42.771	13.413	IT	- , -	- , -	0.068 , -0.200
AME	42.56	12.414	IT	- , -	- , -	-0.482 , -0.098
AMT	42.632	13.286	IT	- , -	- , -	-0.004 , 0.028
AMUR	40.907	16.604	IV	-0.747 , 0.037	- , -	- , -
ANB	43.592	13.507	IT	- , -	- , -	- , 0.287
AND3	40.93	15.333	IT	-0.146 , 0.536	- , -	- , -
ANT	42.418	13.079	IT	- , -	- , -	-0.011 , -0.067
AOI	43.55	13.602	IV	-0.262 , -0.171	- , -	- , -
APEC	43.558	12.42	IV	-0.083 , -0.112	- , -	- , -
APRC	41.757	15.543	IV	-0.185 , 0.180	0.045 , -0.222	- , -
AQA	42.376	13.339	IT	- , -	- , -	0.125 , -0.005
AQF	42.381	13.355	IT	- , -	- , -	0.346 , -0.088
AQG	42.373	13.337	IT	- , -	- , -	0.281 , 0.074
AQK	42.345	13.401	IT	- , -	- , -	0.401 , 0.173
AQM	42.379	13.349	IT	- , -	- , -	-0.104 , -0.161
AQP	42.384	13.369	IT	- , -	- , -	0.180 , 0.093
AQU	42.354	13.405	MN	-0.247 , -0.088	- , -	- , -
AQV	42.377	13.344	IT	- , -	- , -	0.459 , 0.095
ARCI	42.852	11.475	IV	-1.236 , -0.433	- , -	- , -
ARI	41.155	15.09	IT	- , -	- , -	- , 0.254
ARL	41.057	14.543	IT	- , -	- , -	- , -0.601
ARRO	42.579	12.766	IV	- , -	-0.366 , -0.304	- , -
ARVD	43.498	12.942	IV	-0.206 , -0.279	- , -	- , -
ASP	42.848	13.648	IT	- , -	- , -	0.598 , 0.174
ASQU	43.797	11.789	IV	-0.514 , -0.357	- , -	- , -
ASR	41.199	15.563	IT	- , -	- , -	- , 0.369
ASS	43.075	12.604	IT	- , -	- , -	0.465 , -0.012
ASSB	43.043	12.659	IV	0.224 , -0.083	- , -	- , -
AT09	43.314	12.54	TV	- , -	-0.226 , -0.001	- , -
ATBU	43.476	12.548	IV	- , -	-0.239 , -0.271	- , -
ATCC	43.185	12.64	IV	- , -	0.081 , -0.016	0.074 , 0.043
ATFO	43.367	12.571	IV	-0.404 , -0.178	- , -	-0.200 , -0.102
ATI	41.622	13.795	IT	- , -	- , -	- , 0.056
ATLO	43.315	12.407	IV	- , -	-0.501 , -0.431	-0.334 , -0.262
ATMC	43.447	12.193	IV	- , -	-0.161 , -0.424	- , -
ATMI	43.334	12.268	IV	0.336 , 0.107	- , -	- , -
ATN	41.62	13.801	IT	- , -	- , -	0.395 , -0.015
ATPC	43.481	12.457	IV	0.006 , -0.043	- , -	0.134 , -0.089
ATPI	43.451	12.402	IV	- , -	-0.450 , -0.526	- , -
ATRE	43.546	12.264	IV	-0.627 , -0.574	- , -	- , -
ATTE	43.198	12.354	IV	-0.648 , -0.234	- , -	-0.515 , -0.211
ATVO	43.382	12.407	IV	-0.558 , -0.220	- , -	-0.304 , -0.183
AVL	40.923	14.787	IT	- , -	- , -	- , 0.353
AVZ	42.027	13.426	IT	- , -	- , -	0.885 , 0.224

BADI	43.51	12.244	IV	- , -	-0.307 , -0.502	- , -
BCN	40.634	15.382	IT	- , -	- , -	- , -0.189
BDI	44.062	10.597	IV	-0.450 , -0.381	- , -	- , -
BDT	43.707	12.188	IT	- , -	- , -	- , -0.062
BEL3	40.715	15.637	IR	- , -	- , -	- , -0.490
BGI	40.831	15.068	IT	- , -	- , -	-0.257, 0.399
BGR	43.889	11.991	IT	- , -	- , -	- , -0.021
BIOG	41.2	15.133	IV	-0.023 , 0.391	- , -	- , -
BNV	41.118	14.797	IT	- , -	- , -	- , 0.354
BOI	41.481	14.472	IT	- , -	- , -	- , 0.083
BOJ	41.484	14.472	IT	- , -	- , -	- , 0.622
BOR	42.507	13.141	IT	- , -	- , -	0.667 , 0.174
BRB	43.954	11.213	IT	- , -	- , -	- , -0.010
BRIS	44.225	11.767	IV	0.406 , -0.029	- , -	-0.017 , -
BRS	42.324	13.59	IT	- , -	- , -	- , -0.091
BSS	42.19	13.844	IT	- , -	- , -	- , 0.089
BSSO	41.546	14.594	IV	-0.975 , -0.212	- , -	-0.003 , 0.124
BTT2	41.999	13.543	IT	- , -	- , -	- , 0.696
BULG	40.078	15.378	IV	-1.326 , -0.153	- , -	- , -
BVG	42.932	12.611	IT	- , -	- , -	- , 0.729
BVN	41.249	15.342	IT	- , -	- , -	- , 0.095
BZZ	42.337	13.469	IT	- , -	- , -	-0.085 , -0.108
CAAM	40.82	14.141	IV	0.317 , 0.356	- , -	- , -
CADA	43.194	13.761	IV	- , -	- , -	0.915 , 0.489
CAFE	41.028	15.237	IV	-0.540 , 0.086	- , -	- , -
CAFI	43.329	11.966	IV	-0.617 , -0.245	- , -	-0.558 , -0.318
CAFR	42.227	14.347	IV	0.224 , -0.050	- , -	0.593 , 0.013
CAMP	42.536	13.409	IV	-0.807 , -0.297	- , -	- , -
CAPA	41.158	15.817	IV	-0.011 , 0.418	- , -	- , -
CASP	42.791	10.865	IV	-0.992 , -0.390	- , -	- , -
CCT	43.368	12.235	IT	- , -	- , -	- , 0.441
CDCA	43.458	12.234	IV	- , -	- , -	0.850 , 0.254
CDM	42.003	14.199	IT	- , -	- , -	0.067 , -0.097
CDRU	40.49	15.305	IV	-0.893 , -0.166	- , -	- , -
CDS	41.787	14.112	IT	- , -	- , -	0.579 , 0.084
CELB	42.747	10.211	IV	-1.188 , -0.844	- , -	- , -
CER	41.259	15.91	IT	- , -	- , -	- , 0.448
CERA	41.598	14.018	IV	-0.076 , -0.017	- , -	0.323 , -0.079
CERT	41.949	12.982	IV	-0.256 , -0.081	- , -	- , -
CESI	43.005	12.905	IV	-0.369 , -0.254	- , -	- , -
CESX	42.608	12.587	IV	-0.317 , -0.072	- , -	- , -
CFMN	40.833	14.094	IV	0.495 , 0.008	- , -	- , -
CHT	42.37	14.148	IT	- , -	- , -	1.041 , 0.375
CIGN	41.654	14.905	IV	-0.642 , -0.057	- , -	- , -
CIMA	43.305	13.67	IV	- , -	- , -	0.733 , 0.463
CING	43.376	13.195	IV	-0.061 , -0.186	- , -	- , -
CIT	42.594	13.163	IT	- , -	- , -	0.338 , 0.147
CLF	43.037	12.92	IT	- , -	- , -	0.628 , 0.393
CLN	42.085	13.521	IT	- , -	- , -	-0.401 , -0.298
CLO	42.829	13.206	IT	- , -	- , -	0.275 , 0.110
CLT	40.899	15.439	IT	- , -	- , -	- , 0.208
CMB	41.563	14.652	IT	- , -	- , -	- , -0.205
CME	43.954	10.301	IT	- , -	- , -	0.119 , -0.439

CMI	42.85	13.093	IT	- , -	- , -	0.336 , 0.218
CML	40.747	13.901	IT	- , -	- , -	- , 0.495
CMNZ	42.951	13.408	IT	- , -	- , -	0.747 , 0.215
CMPO	44.581	11.806	IV	- , -	- , -	0.717 , 0.348
CMPR	40.318	15.303	IV	-1.362 , -0.119	- , -	- , -
CMR	41.833	14.712	IT	- , -	- , -	- , -0.080
CMSN	40.838	14.182	IV	0.483 , 0.556	- , -	- , -
CNC	41.078	14.025	IT	- , -	- , -	- , 0.624
CNE	42.894	13.153	IT	- , -	- , -	0.513 , 0.046
CNMT	42.456	13.23	IT	- , -	- , -	0.658 , 0.426
CNO	43.142	13.079	IT	- , -	- , -	0.426 , 0.224
COL3	40.687	15.33	IX	-0.003 , 0.345	- , -	- , -
COLB	40.819	14.147	IV	0.860 , 0.109	- , -	- , -
COR1	43.632	13	IV	- , -	- , -	- , 0.312
CPGN	43.801	12.321	IV	- , -	- , -	- , -0.108
CPIS	40.829	14.147	IV	2.139 , 0.667	- , -	- , -
CPOZ	40.821	14.119	IV	0.848 , 0.385	- , -	- , -
CPS	42.272	13.758	IT	- , -	- , -	-0.443 , -0.021
CPT	42.827	12.925	IT	- , -	- , -	0.208 , -0.021
CRAC	40.365	16.435	IV	- , -	-0.001 , 0.004	- , -
CRE	43.619	11.952	IV	-0.542 , -0.346	- , -	- , -
CRM1	43.21	13.058	IV	- , -	- , -	- , 0.322
CRMI	43.796	10.98	IV	-1.554 , -0.760	- , -	- , -
CRO	43.268	11.981	IT	- , -	- , -	- , -0.522
CRTO	40.821	14.422	IV	2.800 , 0.704	- , -	- , -
CSA	43.008	12.591	IT	- , -	- , -	1.427 , 0.539
CSAN	42.9	13.145	IT	- , -	- , -	0.027 , -0.200
CSC	42.719	13.012	IT	- , -	- , -	0.030 , 0.032
CSD	42.754	12.004	IT	- , -	- , -	0.747 , 0.156
CSFT	40.829	14.14	IV	1.659 , 0.178	- , -	- , -
CSG3	40.818	15.463	IX	- , -	- , -	0.313 , 0.469
CSN	44.137	12.241	IT	- , -	- , -	- , 0.078
CSNT	43.473	11.29	IV	-0.903 , -0.417	- , -	- , -
CSO1	42.101	13.088	IT	- , -	- , -	-0.120 , 0.049
CSOB	40.827	14.144	IV	0.556 , 0.246	- , -	- , -
CSP1	43.092	13.205	IV	- , -	- , -	- , -
CSS	41.486	13.823	IT	- , -	- , -	- , -0.072
CTD	42.388	12.948	IT	- , -	- , -	0.389 , 0.143
CTL	43.955	12.736	IT	- , -	- , -	- , 0.275
CTRL	42.598	13.163	IT	- , -	- , -	-0.278 , -0.036
CTS	43.492	12.223	IT	- , -	- , -	- , 0.323
CUC	39.994	15.816	MN	-1.951 , -0.225	- , -	- , -
CVM	42.994	11.282	IT	- , -	- , -	- , -0.359
DUR	41.661	14.457	IT	- , -	- , -	- , -0.155
ED01	42.526	13.093	YR	0.435 , 0.124	- , -	- , -
ED02	42.604	12.929	YR	-0.306 , -0.237	- , -	- , -
ED03	42.603	13.19	YR	0.226 , 0.091	- , -	- , -
ED04	42.574	13.297	YR	-0.321 , -0.183	- , -	- , -
ED05	42.484	13.365	YR	-0.267 , -0.116	- , -	- , -
ED06	42.464	13.228	YR	-0.152 , -0.052	- , -	- , -
ED07	42.628	13.452	YR	-0.147 , -0.204	- , -	- , -
ED08	42.459	13.054	YR	-0.760 , -0.326	- , -	- , -
ED09	42.8	13.424	YR	0.648 , -0.017	- , -	- , -

ED10	42.777	13.141	YR	0.513 , -0.242	- , -	- , -
ED11	42.688	13.033	YR	0.137 , -0.140	- , -	- , -
ED12	42.806	12.977	YR	-0.148 , -0.160	- , -	- , -
ED14	42.445	13.433	YR	-0.201 , -0.147	- , -	- , -
ED15	42.528	13.558	YR	0.331 , -0.098	- , -	- , -
ED16	42.837	13.307	YR	1.108 , 0.381	- , -	- , -
ED17	42.966	13.309	YR	0.545 , -0.045	- , -	- , -
ED18	42.992	13.243	YR	-0.159 , -0.174	- , -	- , -
ED19	42.92	13.139	YR	0.028 , -0.065	- , -	- , -
ED20	42.749	13.435	YR	-0.011 , -0.157	- , -	- , -
ED21	43.03	13.272	YR	-0.267 , -0.174	- , -	- , -
ED22	43.007	13.325	YR	0.933 , 0.215	- , -	- , -
ED23	42.743	13.287	YR	0.478 , 0.208	- , -	- , -
ED24	42.656	13.192	YR	0.160 , -0.001	- , -	- , -
ED25	42.599	13.352	YR	-0.176 , -0.053	- , -	- , -
EL6	43.329	13.102	IV	- , -	- , -	- , -
FAA	42.553	13.537	IT	- , -	- , -	0.807 , 0.065
FAGN	42.266	13.584	IV	0.467 , 0.126	- , -	- , -
FBR	43.344	12.912	IT	- , -	- , -	0.618 , 0.079
FCC	42.755	13.193	IT	- , -	- , -	0.132 , -0.025
FDMO	43.036	13.087	IV	-0.375 , -0.278	- , -	- , -
FEMA	42.962	13.05	IV	- , -	- , -	0.100 , -0.069
FIAM	42.268	13.117	IV	-1.052 , -0.342	- , -	-0.130 , -0.064
FIE	43.807	11.294	IT	- , -	- , -	- , -0.549
FIR	43.774	11.255	IV	-0.304 , -0.191	- , -	- , -
FIU	44.64	11.492	IV	- , -	- , 0.007	- , -
FIU1	43.189	12.932	IV	- , -	- , -	-0.246 , -0.286
FLT	41.893	13.325	IT	- , -	- , -	-0.378 , -0.192
FMG	42.268	13.117	IT	- , -	- , -	-0.158 , -0.107
FMT	43.188	12.933	IT	- , -	- , -	0.910 , 0.051
FNVD	44.168	11.123	IV	-0.169 , -0.112	- , -	- , -
FOC	43.026	12.896	IT	- , -	- , -	0.672 , 0.059
FOCC	42.957	12.708	IT	- , -	- , -	0.478 , 0.223
FOPC	42.97	12.703	IT	- , -	- , -	0.300 , 0.188
FOS	43.015	12.835	IT	- , -	- , -	0.342 , 0.038
FOSV	43.295	12.761	IV	- , -	-0.262 , -0.251	-0.196 , -0.232
FRES	41.974	14.669	IV	-0.305 , -0.112	- , -	- , -
FRON	43.518	12.726	IV	- , -	-0.013 , -0.298	- , -
FROS	43.21	11.156	IV	-0.126 , -0.130	- , -	- , -
FRT	41.693	13.255	IT	- , -	- , -	- , -0.112
FSS	43.69	12.81	IT	- , -	- , -	- , -0.180
FSSB	43.693	12.777	IV	0.678 , 0.193	- , -	- , -
GAG1	43.238	13.067	IV	- , -	- , -	0.895 , 0.233
GATE	41.513	14.91	IV	-0.647 , -0.048	- , -	- , -
GAVE	42.692	12.894	IV	- , -	0.116 , -0.031	- , -
GBB	43.357	12.597	IT	- , -	- , -	0.255 , -0.095
GBC	43.355	12.573	IT	- , -	- , -	-0.346 , -0.321
GBM	43.38	12.497	IT	- , -	- , -	0.572 , 0.381
GBP	43.314	12.589	IT	- , -	- , -	1.180 , 0.579
GIGS	42.453	13.573	IV	-1.277 , -0.616	- , -	- , -
GIUL	41.558	13.255	IV	-0.599 , -0.189	- , -	- , -
GLD	41.509	14.757	IT	- , -	- , -	- , -0.133
GLT	43.233	12.789	IT	- , -	- , -	-0.166 , -0.283

GNU	42.804	12.57	IT	- , -	- , -	0.222 , -0.061
GRD	42.179	14.18	IT	- , -	- , -	0.761 , -0.304
GRN	41.813	13.317	IT	- , -	- , -	-0.210 , -0.067
GROG	43.426	9.892	IV	-1.117 , -0.829	- , -	- , -
GSA	42.421	13.519	IT	- , -	- , -	0.270 , -0.066
GSG	42.46	13.55	IT	- , -	- , -	-1.016 , -0.554
GSN	41.307	14.446	IT	- , -	- , -	- , 0.085
GUAR	41.794	13.312	IV	-0.211 , -0.101	- , -	- , -
GUMA	43.063	13.335	IV	0.624 , 0.309	- , -	0.696 , 0.382
IFOR	40.711	13.855	IV	1.384 , 0.528	- , -	- , -
IMTC	40.721	13.876	IV	-0.961 , -	- , -	- , -
INTR	42.012	13.905	IV	0.039 , 0.012	- , -	-0.607 , 0.092
ISR	41.611	14.236	IT	- , -	- , -	0.637 , 0.159
LAT	41.472	12.907	IT	- , -	- , -	- , 0.173
LATE	42.614	11.804	IV	0.322 , 0.207	- , -	- , -
LAV9	41.678	12.699	IV	0.711 , 0.354	- , -	- , -
LDP	42.039	14.183	IT	- , -	- , -	- , -0.056
LG01	42.622	13.282	XJ	0.061 , -0.131	- , -	- , -
LG02	42.665	13.308	XJ	-0.040 , -0.180	- , -	- , -
LG03	42.457	13.356	XJ	0.818 , 0.002	- , -	- , -
LG04	42.71	13.448	XJ	0.764 , -0.096	- , -	- , -
LG05	42.701	13.635	XJ	0.996 , 0.210	- , -	- , -
LG06	42.621	13.507	XJ	0.400 , -0.059	- , -	- , -
LG07	42.596	13.662	XJ	0.798 , -0.076	- , -	- , -
LG08	42.381	13.662	XJ	1.169 , 0.268	- , -	- , -
LG09	42.448	13.819	XJ	0.576 , 0.100	- , -	- , -
LG10	42.507	13.67	XJ	0.534 , -0.127	- , -	- , -
LG11	42.121	13.336	XJ	-0.222 , -0.430	- , -	- , -
LG12	42.079	13.514	XJ	0.664 , -0.085	- , -	- , -
LG13	42.028	13.65	XJ	0.393 , -0.080	- , -	- , -
LG14	42	13.799	XJ	0.626 , 0.143	- , -	- , -
LG15	42.113	13.814	XJ	-0.126 , -0.195	- , -	- , -
LG16	42.219	13.783	XJ	0.420 , -0.009	- , -	- , -
LG17	42.319	13.777	XJ	0.554 , -0.164	- , -	- , -
LG18	42.13	13.702	XJ	1.249 , 0.300	- , -	- , -
LG19	42.308	13.241	XJ	0.163 , -0.150	- , -	- , -
LG20	42.205	13.255	XJ	0.235 , -0.320	- , -	- , -
LIO3	40.897	15.18	IX	-0.689 , 0.177	- , -	- , -
LMD	44.077	11.707	IV	-0.553 , -0.373	- , -	- , -
LNSS	42.603	13.04	IV	0.202 , 0.012	- , -	- , -
LPEL	42.047	14.183	IV	0.067 , -0.062	- , -	- , -
LRP	41.647	13.587	IV	-0.745 , -0.280	- , -	- , -
LSN	41.853	15.36	IT	- , -	- , -	- , 0.575
LSS	42.558	12.969	IT	- , -	- , -	-0.361 , -0.175
LTA	41.472	12.907	IT	- , -	- , -	- , 0.325
MA9	41.77	12.659	IV	0.353 , 0.148	- , -	- , -
MAON	42.428	11.131	IV	-0.638 , -0.265	- , -	- , -
MATE	40.649	16.704	GE	-0.748 , -0.057	- , -	- , -
MCEL	40.325	15.802	IV	-0.841 , -0.067	- , -	- , -
MCI	41.491	13.813	IV	- , -	-0.070 , -0.033	- , -
MCIV	42.779	11.677	IV	-0.807 , -0.379	- , -	- , -
MCR	43.8	12.448	IT	- , -	- , -	- , 0.111
MCRV	40.783	15.168	IV	-0.322 , 0.126	- , -	- , -

MCS	43.994	12.107	IT	- , -	- , -	- , -0.138
MCT	43.292	13.419	IT	- , -	- , -	- , 0.587
MCV	42.993	13.001	IT	- , -	- , -	0.193 , -0.129
MDAR	43.193	13.143	IV	- , -	- , -	-0.212 , -0.350
MELA	41.706	15.127	IV	-0.079 , 0.239	- , -	- , -
MGAB	42.913	12.112	IV	0.040 , 0.074	- , -	0.018 , -0.044
MGR	40.138	15.554	IV	-1.658 , -0.317	- , -	- , -
MIDA	41.642	14.254	IV	-0.292 , -0.181	- , -	-0.612 , -0.376
MIGL	40.604	16.441	IV	-0.303 , -	- , -	- , -
MML1	43.113	12.972	IV	- , -	-0.340 , -0.300	- , -
MMN	39.891	15.99	IV	-2.473 , -0.631	- , -	- , -
MMO	42.899	13.327	IT	- , -	- , -	0.239 , 0.092
MMO1	42.899	13.327	IV	- , -	-0.023 , -0.056	0.108 , -0.091
MMP	42.249	12.749	IT	- , -	- , -	-0.041 , 0.002
MMP1	42.249	12.748	IT	- , -	- , -	0.129 , 0.031
MMUR	43.442	12.997	IV	- , -	- , -	0.573 , 0.092
MND	41.64	15.891	IT	- , -	- , -	-0.216 , 0.128
MNF	43.06	13.184	IT	- , -	- , -	-0.437 , -0.325
MNG	41.703	15.959	IT	- , -	- , -	- , 0.564
MNN	41.634	15.911	IT	- , -	- , -	0.370 , 0.351
MNS	42.385	12.681	IV	-0.222 , -0.154	- , -	- , -
MNT	43.14	11.183	IT	- , -	- , -	0.183 , -0.330
MNT3	40.837	15.007	IX	-0.540 , -0.157	- , -	- , -
MNTP	43.137	13.469	IV	- , -	- , -	0.586 , 0.299
MOCL	44.005	11.181	IV	- , -	-0.895 , -0.168	- , -
MOCO	41.37	15.158	IV	-1.150 , -0.089	- , -	- , -
MODR	41.146	13.878	IV	-0.612 , 0.069	- , -	- , -
MOMA	43.801	12.568	IV	-0.086 , -0.094	- , -	0.059 , 0.003
MPAG	43.629	12.759	IV	- , -	-0.271 , -0.400	0.089 , 0.150
MRB1	41.123	14.968	IV	-0.086 , 0.261	- , -	- , 0.805
MRH	41.342	16.194	IT	- , -	- , -	- , 0.645
MRLC	40.756	15.489	IV	-0.826 , -0.078	- , -	- , -
MRR	44.064	11.603	IT	- , -	- , -	- , -0.307
MRT	40.79	14.753	IT	- , -	- , -	- , 0.737
MRVN	41.061	16.196	IV	-0.956 , 0.005	- , -	- , -
MSAG	41.712	15.91	IV	0.109 , 0.326	- , -	- , -
MSC	42.526	13.346	IT	- , -	- , -	-0.038 , 0.093
MSCT	42.527	13.351	IT	- , -	- , -	0.032 , 0.099
MTC	41.491	13.815	IT	- , -	- , -	0.806 , 0.243
MTCE	42.023	12.742	IV	-0.538 , -0.131	- , -	- , -
MTCL	42.994	12.999	IT	- , -	- , -	-0.222 , -0.282
MTFT	42.942	13.343	IT	- , -	- , -	-0.019 , -0.142
MTL	43.249	13.008	IT	- , -	- , -	0.715 , 0.194
MTL1	43.257	13.01	IV	- , -	- , -	0.814 , 0.263
MTMR	40.918	15.003	IV	- , -	- , -	- , 0.097
MTR	42.524	13.245	IT	- , -	- , -	- , 0.021
MTRA	42.757	13.397	IV	- , -	0.027 , -0.133	- , -
MTRZ	44.313	11.425	IV	0.232 , 0.004	- , -	- , -
MTSN	40.266	15.752	IV	-1.581 , -0.371	- , -	- , -
MURB	43.263	12.525	IV	0.630 , 0.234	- , -	0.664 , 0.245
MVB	42.962	12.257	IT	- , -	- , -	0.112 , -0.264
MVO	42.581	13.625	IT	- , -	- , -	0.524 , -0.051
NARO	43.611	12.581	IV	-0.435 , -	- , -	- , -

NCR	43.112	12.785	IT	- , -	- , -	- , 0.152
NOR	42.792	13.092	IT	- , -	- , -	0.523 , 0.303
NRC	42.793	13.096	IT	- , -	- , -	0.231 , 0.209
NRCA	42.834	13.114	IV	0.602 , 0.029	- , -	0.513 , 0.061
NRN	42.516	12.519	IT	- , -	- , -	-0.140 , -0.024
NSC3	40.847	15.122	IX	-0.601 , 0.206	- , -	- , -
OFFI	42.935	13.686	IV	0.568 , 0.327	- , -	- , -
OPI	41.776	13.83	IT	- , -	- , -	- , -0.143
ORC	41.954	13.642	IT	- , -	- , -	0.281 , -0.087
OSSC	43.524	11.246	IV	-0.421 , -0.180	- , -	- , -
PALZ	40.944	15.96	IV	0.028 , 0.445	- , -	- , -
PAN	43.006	12.144	IT	- , -	- , -	-0.062 , -0.238
PAOL	41.031	14.567	IV	-0.673 , -0.064	- , -	- , -0.190
PARC	43.649	12.239	IV	-0.316 , -0.207	- , -	- , -
PBN	43.064	13.082	IT	- , -	- , -	0.091 , -0.100
PCB	42.557	13.336	IT	- , -	- , -	0.279 , -0.010
PCRO	43.608	13.532	IV	- , -	- , -	0.751 , 0.335
PDM	41.355	14.385	IT	- , -	- , -	-0.210 , -0.187
PESA	43.941	12.84	IV	0.518 , 0.081	- , -	- , -
PGG	42.322	13.54	IT	- , -	- , -	0.726 , 0.172
PGN	41.452	13.792	IT	- , -	- , -	- , 0.703
PIEI	43.536	12.535	IV	-0.246 , -0.317	- , -	-0.362 , -0.312
PIGN	41.2	14.18	IV	-0.977 , -0.165	- , -	- , -
PII	43.722	10.525	IV	0.704 , 0.031	- , -	- , -
PIO1	43.178	12.984	IV	- , -	- , -	-0.180 , -0.191
PIT	43.99	10.944	IT	- , -	- , -	0.234 , -0.214
PLMA	44.05	9.854	IV	-0.953 , -0.877	- , -	- , -
PLS	42.084	12.763	IT	- , -	- , -	-0.094 , -0.073
PNC	42.847	11.693	IT	- , -	- , -	- , 0.064
PNN	43.818	12.263	IT	- , -	- , -	- , 0.266
POFI	41.717	13.712	IV	-0.649 , -0.238	- , -	0.104 , 0.316
PP3	43.378	13.609	IV	- , -	0.644 , 0.039	0.863 , 0.607
PRE	42.879	13.033	IT	- , -	- , -	-0.141 , -0.060
PRG	43.111	12.325	IT	- , -	- , -	- , -0.410
PRGP	43.112	12.388	IT	- , -	- , -	- , 0.304
PRZ	41.38	14.112	IT	- , -	- , -	- , 0.616
PSB1	41.223	14.811	IV	-0.574 , 0.049	- , -	- , -
PSC	41.812	13.789	IT	- , -	- , -	-0.011 , -0.001
PTF	41.696	14.702	IT	- , -	- , -	- , 0.093
PTI	43.067	13.657	IT	- , -	- , -	0.806 , 0.371
PTL	43.427	12.449	IT	- , -	- , -	0.188 , -0.018
PTQR	42.022	13.401	IV	-0.852 , -0.320	- , -	- , -
PTRJ	41.364	14.529	IV	-0.405 , -0.020	- , -	- , -
PVS	43.669	12.044	IT	- , -	- , -	0.335 , -0.177
PZI	42.437	13.327	IT	- , -	- , -	-0.060 , -0.047
PZI1	42.436	13.326	IT	- , -	- , -	0.048 , 0.021
PZUN	40.646	15.807	BA	-0.213 , -0.045	- , -	- , -
PZZ	41.674	14.036	IT	- , -	- , -	- , -0.195
RAVA	44.756	11.119	IV	- , -	0.072 , -0.779	- , -
RCC	41.289	13.98	IT	- , -	- , -	- , 0.440
RCCR	41.839	14.085	IT	- , -	- , -	- , 0.503
RCG	42.292	12.206	IT	- , -	- , -	- , 0.171
RDD	43.491	11.385	IT	- , -	- , -	- , -0.222

RDG	41.926	15.879	IT	- , -	- , -	0.658 , 0.460
RDM3	40.875	15.536	IX	-0.118 , 0.460	- , -	- , -
RDP	41.758	12.717	IV	0.656 , 0.284	- , -	- , -
RFC	42.536	13.409	IT	- , -	- , -	-0.237 , -0.306
RM01	42.277	13.336	IV	- , -	- , -	0.017 , -0.202
RM02	42.343	13.328	IV	- , -	- , -	-0.282 , -0.242
RM03	42.274	13.472	IV	- , -	- , -	-0.705 , -0.418
RM04	42.188	13.451	IV	- , -	- , -	-0.214 , -0.229
RM05	42.439	13.259	IV	- , -	- , -	0.133 , 0.005
RM06	42.378	13.244	IV	- , -	- , -	0.113 , -0.182
RM07	42.405	13.407	IV	- , -	- , -	0.965 , 0.240
RM08	42.372	13.505	IV	- , -	- , -	-0.109 , -0.295
RM09	42.436	13.186	IV	- , -	- , -	-0.412 , -0.371
RM10	42.509	13.186	IV	- , -	- , -	0.312 , -0.042
RM11	42.538	13.277	IV	- , -	- , -	-0.139 , -0.294
RM12	42.262	13.392	IV	0.967 , 0.291	- , -	- , -
RM13	42.182	13.581	IV	- , -	- , -	-0.155 , -0.207
RM14	42.345	13.572	IV	- , -	- , -	-0.117 , -0.274
RM15	42.282	13.245	IV	1.306 , 0.297	- , -	- , -
RM16	42.235	13.532	IV	0.839 , 0.086	- , -	- , -
RM18	42.55	13.532	IV	- , -	- , -	- , -0.117
RM20	42.525	13.126	IV	- , -	- , -	- , -0.228
RM21	42.628	13.142	IV	- , -	- , -	- , -0.233
RM22	42.444	13.049	IV	- , -	- , -	- , -0.143
RM24	42.171	13.472	IV	- , -	- , -	- , -0.219
RM25	42.622	13.282	IV	- , -	- , -	- , -0.033
RM26	42.457	13.356	IV	- , -	- , -	- , 0.539
RM27	42.302	13.68	IV	- , -	- , -	- , -0.299
RM28	42.402	13.549	IV	- , -	- , -	- , 0.015
RM29	42.561	13.202	IV	- , -	0.013 , -0.008	- , -
RM30	42.533	13.093	IV	- , -	- , -	- , -0.091
RM31	42.702	13.233	IV	- , -	- , -	- , -0.054
RM32	42.57	13.293	IV	- , -	-0.359 , -0.332	- , -
RM33	42.509	13.215	IV	- , -	-0.219 , -0.298	-0.026 , -0.038
RMCL	41.914	12.454	IT	- , -	- , -	- , 0.067
RMMM	41.923	12.453	IT	- , -	- , -	- , 0.444
RMP	41.811	12.702	IV	0.285 , 0.110	- , -	- , -
RMVT	41.956	12.486	IT	- , -	- , -	- , 0.761
RNI2	41.703	14.152	IV	0.027 , 0.052	- , -	- , -
ROM9	41.828	12.516	IV	0.935 , 0.536	- , -	0.551 , 0.651
RQT	42.813	13.311	IT	- , -	- , -	0.575 , 0.086
RSF3	40.964	15.176	IX	-0.604 , 0.160	- , -	- , -
RSM	43.93	12.45	IV	- , -	- , -	- , 0.063
RSM2	43.938	12.445	IV	0.208 , 0.153	- , -	- , -
RTI	42.431	12.829	IT	- , -	- , -	0.953 , 0.590
SACR	41.397	14.706	IV	-0.751 , -0.012	- , -	0.046 , 0.156
SACS	42.849	11.91	IV	-0.517 , -0.152	- , -	-0.127 , -0.011
SAG	40.932	15.188	IT	- , -	- , -	0.257 , 0.708
SAMA	41.78	12.592	IV	0.011 , -0.006	- , -	- , -
SBC	41.913	13.106	IT	- , -	- , -	0.423 , -0.336
SBT	42.934	13.86	IT	- , -	- , -	- , 0.491
SCF	42.265	13.998	IT	- , -	- , -	1.055 , 0.306
SCHE	43.404	12.668	IT	- , -	- , -	-0.134 , -0.278

SCHR	40.199	16.076	IV	- , -	-1.459 , -0.425	- , -
SCL3	40.695	15.511	IR	- , -	- , -	- , -0.605
SCN	41.919	13.872	IT	- , -	- , -	0.264 , 0.050
SCO	42.363	13.266	IT	- , -	- , -	- , 0.559
SDG	41.843	15.559	IT	- , -	- , -	- , 0.008
SDM	42.289	13.558	IT	- , -	- , -	0.209 , -0.001
SEF1	43.147	12.948	IV	- , -	- , -	0.895 , 0.132
SEI	44.054	11.359	IV	0.196 , -0.119	- , -	- , -
SENI	43.705	13.233	IV	- , -	- , -	0.828 , 0.397
SF11	42.869	11.679	TV	-0.526 , -0.270	- , -	- , -
SF13	42.818	11.62	TV	-0.654 , -0.314	- , -	- , -
SF14	42.755	11.615	TV	-0.548 , -0.225	- , -	- , -
SFI	43.905	11.847	IV	- , -	-0.623 , -0.749	- , -
SGG	41.387	14.379	IV	-0.534 , -0.087	- , -	- , -
SGMA	41.685	14.964	IT	- , -	- , -	- , 0.279
SGPA	41.688	14.963	IT	- , -	- , -	- , 0.025
SGRT	41.755	15.744	IV	-0.146 , 0.279	- , -	- , -
SGSC	41.689	14.958	IT	- , -	- , -	- , 0.090
SGTA	41.135	15.365	IV	-0.533 , 0.068	- , -	- , -
SIG	43.331	12.741	IT	- , -	- , -	0.362 , -0.124
SIRI	40.182	15.868	IV	-1.383 , -0.317	- , -	- , -
SLCN	40.39	15.633	IV	-0.248 , 0.171	- , -	- , -
SLD	43.874	12.674	IT	- , -	- , -	- , 0.179
SLO	42.9	12.953	IT	- , -	- , -	-0.290 , -0.135
SMA1	42.631	13.335	IV	- , -	0.002 , -0.050	- , -
SMP	44.064	10.804	IT	- , -	- , -	- , -0.536
SNAL	40.925	15.209	IV	-0.418 , -	- , -	- , -
SNG	43.686	13.226	IT	- , -	- , -	- , 0.379
SNI	42.632	12.554	IT	- , -	- , -	0.593 , 0.384
SNM	43.934	12.449	IT	- , -	- , -	- , 0.314
SNN	41.832	15.571	IT	- , -	- , -	0.392 , 0.181
SNO	43.037	13.304	IT	- , -	- , -	-0.063 , -0.034
SNR3	40.736	15.193	IX	-0.029 , 0.424	- , -	- , -
SNS1	43.574	12.131	IT	- , -	- , -	0.827 , 0.454
SNTG	43.255	12.941	IV	-0.385 , -0.353	- , -	-0.357 , -0.396
SORA	41.715	13.606	IT	- , -	- , -	- , 0.127
SPC	42.743	12.739	IT	- , -	- , -	-0.185 , -0.154
SPD	42.515	13.371	IT	- , -	- , -	-0.055 , 0.008
SPM	42.723	12.751	IT	- , -	- , -	0.756 , 0.143
SPO	42.734	12.741	IT	- , -	- , -	-0.025 , -0.236
SPO1	42.734	12.736	IT	- , -	- , -	0.658 , 0.390
SPT1	41.458	14.493	IT	- , -	- , -	0.610 , 0.325
SRES	42.237	12.51	IV	-0.641 , -0.199	- , -	- , -
SRL	43.518	13.619	IT	- , -	- , -	0.664 , 0.081
SRN3	40.486	15.458	IX	-1.189 , 0.010	- , -	- , -
SSB3	41.078	15.229	IX	-1.099 , 0.420	- , -	- , -
SSC	42.875	11.877	IT	- , -	- , -	-0.391 , -0.246
SSFR	43.436	12.782	IV	0.617 , 0.056	- , -	0.951 , 0.172
SSG	43.57	12.146	IT	- , -	- , -	0.423 , 0.353
SSM1	43.229	13.177	IV	- , -	- , -	0.120 , -0.043
SSO	43.571	12.154	IT	- , -	- , -	-0.501 , 0.072
SSR	41.691	15.374	IT	- , -	- , -	- , 0.282
SSV	41.681	15.386	IT	- , -	- , -	- , 0.521

STF	43.908	11.794	IT	- , -	- , -	- , -0.319
STG	41.566	14.231	IT	- , -	- , -	- , 0.286
STS	43.942	11.905	IT	- , -	- , -	- , -0.170
SUL	42.09	13.934	IT	- , -	- , -	-0.089 , -0.128
SULA	42.073	13.917	IT	- , -	- , -	0.737 , 0.522
SULC	42.068	13.909	IT	- , -	- , -	0.497 , 0.458
SULP	42.085	13.927	IT	- , -	- , -	0.941 , 0.531
T0101	42.331	13.303	IV	- , -	- , -	0.145 , -0.085
T0102	42.397	13.314	IV	- , -	- , -	-0.206 , -0.230
T0104	42.36	13.338	IV	0.172 , 0.052	- , -	-0.393 , 0.037
T0105	42.311	13.463	IV	- , -	- , -	-0.264 , -0.418
T0106	42.307	13.384	IV	- , -	- , -	0.021 , -0.174
T0107	42.473	13.248	IV	- , -	- , -	0.442 , 0.066
T0110	42.226	13.779	IV	0.055 , 0.091	- , -	0.388 , 0.121
T0203	41.619	13.721	IV	- , -	- , -	- , -0.922
T0402	43.221	13.406	IV	- , -	- , -	0.503 , -
T1011	41.36	14.417	IV	- , -	- , -	- , 0.048
T1012	41.262	14.497	IV	- , -	- , -	- , 0.373
T1101	41.475	14.536	IV	- , -	- , -	0.410 , 0.320
T1201	42.657	13.251	IV	- , -	- , -	0.043 , 0.077
T1204	42.676	13.317	IV	- , -	- , -	- , -
T1211	42.533	12.855	IV	- , -	- , -	0.138 , 0.019
T1212	42.752	13.045	IV	- , -	- , -	-0.418 , -0.071
T1213	42.725	13.126	IV	- , -	- , -	-0.308 , -0.113
T1214	42.76	13.209	IV	- , -	- , -	-0.465 , -0.182
T1215	42.802	12.869	IV	- , -	- , -	-0.644 , -0.360
T1216	42.891	13.019	IV	- , -	- , -	-0.131 , -0.058
T1217	42.712	12.931	IV	- , -	- , -	-0.346 , -0.186
T1218	42.67	13.115	IV	- , -	- , -	-0.121 , -0.023
T1219	43.056	13.005	IV	- , -	- , -	0.302 , -0.237
T1220	43.11	13.089	IV	- , -	- , -	0.765 , 0.324
T1221	42.861	12.847	IV	- , -	- , -	-0.631 , -0.350
T1222	42.401	13.037	IV	- , -	- , -	- , -0.095
T1241	42.856	13.431	IV	-0.305 , -0.162	-0.197 , -0.245	0.009 , -0.020
T1242	42.829	13.204	IV	-0.058 , -0.012	- , -	-0.137 , 0.020
T1243	42.697	13.448	IV	0.588 , 0.150	- , -	0.454 , -0.042
T1244	42.757	13.298	IV	- , -	- , -	0.171 , 0.073
T1245	42.857	13.188	IV	0.288 , 0.043	- , -	0.260 , 0.029
T1246	42.583	13.493	IV	-0.161 , -0.116	- , -	- , -
T1247	42.442	13.298	IV	0.331 , 0.023	- , -	- , -
T1256	43.006	13.226	IV	-0.479 , -0.240	- , -	-0.411 , -0.117
T1299	42.634	13.282	IV	- , -	- , -	-0.203 , -0.109
TER	42.657	13.689	IT	- , -	- , -	0.404 , 0.156
TERO	42.623	13.604	IV	0.077 , -0.095	- , -	-0.301 , -0.187
TLN	43.216	13.258	IT	- , -	- , -	0.805 , 0.296
TLS	41.222	14.53	IT	- , -	- , -	0.568 , 0.196
TMO	41.989	14.975	IT	- , -	- , -	- , 0.464
TOD	42.738	12.387	IT	- , -	- , -	0.354 , 0.268
TOLF	42.064	12	IV	-0.586 , -0.214	- , -	- , -
TRE	42.876	12.736	IT	- , -	- , -	0.608 , 0.273
TRE1	43.311	13.313	IV	- , -	- , -	0.606 , 0.328
TREM	42.123	15.51	IV	0.133 , 0.261	- , -	- , -
TRIF	43.115	10.903	IV	-0.602 , -0.451	- , -	- , -

TRIV	41.767	14.55	IV	-0.386 , -0.083	- , -	- , -
TRL	42.461	12.932	IT	- , -	- , -	0.999 , 0.377
TRN1	42.558	12.646	IT	- , -	- , -	-0.107 , -0.068
TRTR	42.808	13.914	IV	0.919 , 0.488	- , -	- , -
TRV	41.783	14.551	IT	- , -	- , -	- , -0.130
TSC	42.423	11.87	IT	- , -	- , -	- , 0.189
TVR	43.712	11.219	IT	- , -	- , -	- , -0.225
UMB	43.254	12.256	IT	- , -	- , -	0.171 , -0.215
UMBT	43.304	12.344	IT	- , -	- , -	- , 0.290
UST	42.942	13.125	IT	- , -	- , -	0.391 , -0.029
VAGA	41.415	14.234	IV	-0.230 , -0.036	- , -	0.044 , -0.013
VAL	43.159	12.602	IT	- , -	- , -	0.565 , 0.025
VARP	40.817	14.41	IV	0.054 , -	- , -	- , -
VBKN	40.83	14.43	IV	0.507 , 0.421	- , -	- , -
VCEL	42.395	13.841	IV	- , -	0.301 , -0.072	- , -
VCRE	40.819	14.431	IV	0.364 , 0.506	- , -	- , -
VENT	40.795	13.422	IV	- , -	-0.053 , -0.013	- , -
VIE	41.877	16.165	IT	- , -	- , -	0.420 , 0.317
VITU	41.183	14.63	IV	-0.193 , 0.137	- , -	- , -
VIVA	41.75	12.77	IV	0.655 , 0.226	- , -	- , -
VLL	41.67	12.773	IT	- , -	- , -	- , 0.166
VLN	43.143	11.895	IT	- , -	- , -	- , 0.453
VNF1	41.48	14.05	IT	- , -	- , -	- , 0.782
VSD	41.881	16.17	IT	- , -	- , -	0.531 , 0.412
VSE	42.122	14.707	IT	- , -	- , -	- , 0.276
VTIR	40.806	14.424	IV	-0.694 , -0.040	- , -	- , -
VULT	40.955	15.616	IV	0.027 , 0.240	- , -	- , -
VVDG	40.836	14.424	IV	0.066 , 0.170	- , -	- , -
VVLD	41.87	13.623	IV	-0.376 , -0.169	- , -	- , -
ZCCA	44.351	10.976	IV	-0.471 , -0.305	- , -	- , -

Table S1: Station used for the calibration of the Ramones model: S and Z are the station correction coefficient of Eq. (1) and Eq. (2).

Parameters	**Mean ± Stand. dev.**		**Parameters**	**Mean ± Stand. dev.**	
A	-10.639 ± 0.124		**D**	-13.078 ± 0.027	
B	1.064 ± 0.001		**F**	0.801 ± 0.008	
Parameters	**Values**	**Stand. dev.**	**Parameters**	**Values**	**Stand. dev.**
C_1	2,189	0,504	G_1	0,315	0,115
C_2	0,000	0,000	G_2	0,000	0,000
C_3	0,308	0,147	G_3	0,000	0,034
C_4	0,103	0,128	G_4	-0,061	0,03
C_5	-0,028	0,128	G_5	-0,161	0,028
C_6	-0,111	0,125	G_6	-0,180	0,029
C_7	-0,178	0,125	G_7	-0,197	0,026
C_8	-0,27	0,130	G_8	-0,264	0,028
C_9	-0,437	0,123	G_9	-0,288	0,028
C_{10}	-0,508	0,126	G_{10}	-0,337	0,026
C_{11}	-0,576	0,126	G_{11}	-0,378	0,028
C_{12}	-0,709	0,123	G_{12}	-0,418	0,025
C_{13}	-0,812	0,122	G_{13}	-0,482	0,025
C_{14}	-0,946	0,124	G_{14}	-0,523	0,026
C_{15}	-1,053	0,123	G_{15}	-0,559	0,025
C_{16}	-1,176	0,123	G_{16}	-0,630	0,025
C_{17}	-1,319	0,124	G_{17}	-0,682	0,024
C_{18}	-1,428	0,124	G_{18}	-0,733	0,024
C_{19}	-1,538	0,124	G_{19}	-0,804	0,025
C_{20}	-1,666	0,124	G_{20}	-0,865	0,025
C_{21}	-1,745	0,124	G_{21}	-0,909	0,024
C_{22}	-1,858	0,122	G_{22}	-0,985	0,024
C_{23}	-1,946	0,125	G_{23}	-1,021	0,024
C_{24}	-2,055	0,123	G_{24}	-1,067	0,024
C_{25}	-2,167	0,125	G_{25}	-1,132	0,025
C_{26}	-2,303	0,124	G_{26}	-1,195	0,024
C_{27}	-2,408	0,124	G_{27}	-1,238	0,025
C_{28}	-2,503	0,125	G_{28}	-1,310	0,024

C_{29}	-2,625	0,123	G_{29}	-1,360	0,025
C_{30}	-2,694	0,124	G_{30}	-1,423	0,024
C_{31}	-2,798	0,124	G_{31}	-1,479	0,024
C_{32}	-2,891	0,124	G_{32}	-1,545	0,025
C_{33}	-2,974	0,124	G_{33}	-1,634	0,024
C_{34}	-3,093	0,124	G_{34}	-1,684	0,025
C_{35}	-3,281	0,124	G_{35}	-1,747	0,024
C_{36}	-3,334	0,124	G_{36}	-1,834	0,025
C_{37}	-3,488	0,124	G_{37}	-1,870	0,024
C_{38}	-3,559	0,125	G_{38}	-1,924	0,025
C_{39}	-3,747	0,124	G_{39}	-1,983	0,025
C_{40}	-3,799	0,125	G_{40}	-2,004	0,024
C_{41}	-3,902	0,125	G_{41}	-2,038	0,026
C_{42}	-3,990	0,126	G_{42}	-2,081	0,025
C_{43}	-4,142	0,126	G_{43}	-2,125	0,026
C_{44}	-4,241	0,126	G_{44}	-2,160	0,024
C_{45}	-4,334	0,124	G_{45}	-2,160	0,025
C_{46}	-4,434	0,126	G_{46}	-2,205	0,025
C_{47}	-4,515	0,122	G_{47}	-2,252	0,026
C_{48}	-4,64	0,126	G_{48}	-2,298	0,025
C_{49}	-4,652	0,124	G_{49}	-2,369	0,027
C_{50}	-4,936	0,157	G_{50}	-2,381	0,044

Table S2: Regression parameters of Eq. (1) and Eq. (2) with their standard deviations for the calibration dataset.